Article

Development of Allosteric Hydrazide-Containing Class I Histone Deacetylase Inhibitors for Use in Acute Myeloid Leukemia

Jesse McClure, Cheng Zhang, Elizabeth Inks, Yuri K. Peterson, Jiaying Li, and C. James Chou

J. Med. Chem., **Just Accepted Manuscript** • DOI: 10.1021/acs.jmedchem.6b01385 • Publication Date (Web): 18 Oct 2016

Development of Allosteric Hydrazide-Containing Class I Histone Deacetylase Inhibitors for Use in Acute Myeloid Leukemia

*Jesse J. McClure‡, Cheng Zhang‡, Elizabeth S. Inks, Yuri Peterson, Jiaying Li, C. James Chou**

Department of Drug Discovery and Biomedical Sciences, South Carolina College of Pharmacy, Medical University of South Carolina, Charleston, South Carolina 29425, USA

Keywords: Histone Deacetylases, HDAC, Hydrazide, Allosteric, Acute Myeloid Leukemia, Glucuronidation, Michaelis-Menten.

ABSTRACT

One of the biggest hurdles yet to be overcome for the continued improvement of Histone Deacetylase (HDAC) inhibitors is finding alternative motifs equipotent to the classic and ubiquitously used hydroxamic acid. The N-hydroxyl group of this motif is highly subject to sulfation/glucoronidation-based inactivation in humans; compounds containing this motif require much higher dosing in clinic to achieve therapeutic concentrations. With the goal of developing a second generation of HDAC inhibitors, lacking this hydroxamate, we designed a series of potent and selective class I HDAC inhibitors using a hydrazide motif. These inhibitors are impervious to glucuronidation and demonstrate allosteric inhibition. In vitro and ex vivo

characterization of our lead analogs' efficacy, selectivity, and toxicity profiles demonstrate they possess low nanomolar activity against models of Acute Myeloid Leukemia (AML) and are at least 100-fold more selective for AML than solid immortalized cells such as HEK293 or human peripheral blood mononuclear cells.

INTRODUCTION

Histone Deacetylases (HDAC) are a collective of evolutionarily conserved enzymes that are capable of removing acyl-based post translational modifications (PTMs) from ε-nitrogens of lysine residues of histones and other proteins.[1] The 11 identified human HDACs are phylogenetically subdivided into four classes: class I, IIa, IIb, and IV, with class III being the Sirtuin family of enzymes.[2] Of these enzymes, only HDACs 1, 2, 3, and 6, members of the class I and IIb families, have shown biologically relevant deacetylation ability.[3] The canonical targets of HDACs 1, 2, and 3 are acetylated histones H3 (HH3) and H4 (HH4), whereas HDAC6 activity is the sole controller of tubulin acetylation.[4-6]

Inhibition of HDACs 1, 2, 3, and 6 is a promising pathway for treating hematologic cancers in clinic, with FDA approvals of HDAC inhibitors for the treatment of T-cell lymphoma and Multiple Myeloma (MM) (**Chart 1**). Additionally, selective HDAC inhibitors have shown great promise in treating pre-clinical models of cognitive dysfunction and inflammatory-mediated diseases.[7-19] However, despite their clinical successes and increasing promise as novel therapies in a multitude of diseases, approved HDAC inhibitors are commonly associated with dose-limiting toxicities.[20-34] The hydroxamate group, until the FDA approval of vorinostat, was considered to be an undesirable motif in medicinal chemistry. The non-selective metal chelating properties of the hydroxamate are what allow it to bind the catalytic zinc metal that HDACs rely

on, but also cause compounds containing these groups to be associated with many undesirable effects secondary to non-targeted active site metal chelation.[35] While all FDA approved inhibitors demonstrate very strong efficacy in the sub-micromolar range, the doses given in clinic are relatively much higher. The reason for this increased required dose, and the subsequent side effects due to off-target effects, could be in part to a metabolic inactivation of some of these compounds. The hydroxamic acid that is present on three of the four FDA approved HDAC inhibitors, vorinostat, panobinostat, and belinostat, is known to be sulfated or glucuronidated extensively, specifically by UDP glucuronosyltransferase 1A1.[36-39] In the case of vorinostat, the process of glucuronidation has been demonstrated to abrogate its HDAC inhibition activity, and is further evidenced with its issues concerning achieving therapeutic concentrations in clinic.[36] As belinostat and panobinostat also share this hydroxamic acid motif, and have subsequently been shown to be glucuronidated in vivo, a safe assumption can be made that this metabolism causes inactivation for these compounds as well.

Attempts to generate novel, non-hydroxamic acid metal-chelating motifs have resulted in the use of *ortho*-aminoanilide-based HDAC inhibitors, most notably MS-275 (entinostat). However, the benzylic primary amine of this motif is also subject to glucuronidation-based inactivation.[40] Further, this inhibitor was shown to be hepatotoxic in mice.[41] In a more recent attempt to generate non-hydroxamic acid metal-chelating motifs, Wang and colleagues demonstrated a novel, potent, class I HDAC-specific inhibitor series based around a hydrazide motif.[42] Their synthetically refined, lead analog from their initial publication possessed 60 nM HDAC3 inhibition, 500 nM and 100 nM for HDACs 1 and 2 respectively, and at least 20 fold selectivity for class I HDACs compared to HDAC6. With slightly better potency than the similarly selective *ortho*-aminoanilide -based inhibitor entinostat, and containing a novel moiety that

would not likely be subject to glucuronidation/sulfation, we postulated a more potent series of class I selective inhibitors could be generated using hydrazide rather than hydroxamic acid or a benzylic amine. Herein we report on a series of nanomolar to picomolar hydrazide containing HDAC inhibitors, the most potent of which display nanomolar efficacy as single agents in leukemia-based ex vivo models. Further, these compounds are impervious to glucuronidation, inhibit class I HDACs via an allosteric mechanism, display superior, selective toxicity profiles compared to panobinostat at equivalent concentrations in peripheral blood mononuclear cells (PBMCs), and demonstrate greater than 100-fold selectivity toward killing Acute Myeloid Leukemia (AML) when compared to solid tumor cells such as HEK293. This combination of potency, novel inhibition mechanism, and inability to be inactivated via glucuronidation and likely sulfation, and selective toxicity toward leukemia cells make for promising candidates in the treatment of AML.

RESULTS

The goal of our structure-activity relationship studies for the hydrazide-based compounds was to develop a potent and selective inhibitor of class I HDACs, with particular emphasis on HDAC3 inhibition. HDAC3 has shown increasing promise as a novel target to combat leukemia as its inhibition controls hematopoiesis.[43] As such, lead analogs from these studies were tested in pre-clinical leukemia models to determine efficacy and tested against solid tumor models and PBMCs to demonstrate selectivity.

Chemistry of butylhydrazide analogs. We began our structure-activity relationship studies by attempting to identify an ideal substituent for the carbonyl of the hydrazide motif. As shown in **Scheme 1**, we began with either an aromatic carboxylic acid, acyl chloride, or ester. Using commercially available starting materials, we generated the corresponding hydrazide molecule through reactions a, b, and c, depending on the composition of the starting molecule. Target hydrazide compounds were reacted with butylaldehyde to generate the compound of interest. Carboxylic acids were reacted with oxalyl chloride in methylene chloride with catalytic amounts of dimethylformamide (**Scheme 1**, reaction a). The resulting acyl chloride, or commercially purchased acyl chlorides were stirred in methanol to give the corresponding methyl ester (**Scheme 1**, reaction b). The generated or commercially purchased methyl esters were refluxed in methanol with a hydrazine water salt to generate a hydrazide of interest (**Scheme 1**, reaction c). The resulting compounds were then refluxed in ethanol in the presence of magnesium sulfate and butylaldehyde followed by a reduction with sodium cyanoborohydride in acidified methanol to give the desired products **1a**-**1l** (**Scheme 1**, reactions d and e). A notable exception to this scheme was the synthesis of **1d**, which was unable to be esterified from the commercially available corresponding acyl chloride until the addition of two equivalents of triethylamine. Additionally, compound **1i** spontaneously formed the corresponding pyrazolidinone when reacted with the hydrazine salt due to the presence of an unsaturated bond alpha to the ester carbonyl. Instead, the carboxylic acid starting material was reacted with HOBt and DCC in acetonitrile. The resulting intermediate was reacted with the hydrazine water salt in acetonitrile to yield the corresponding hydrazide. Lastly, compound **1l** was the result of reacting methyl 4-(aminomethyl)benzoate with benzoyl chloride to generate the methyl ester corresponding to **1l**. From here, the reaction carried on as shown in **Scheme 1**, reactions d and e.

HDAC inhibition of series 1 inhibitors. With the primary goal of designing a potent and ideally selective series inhibitor of class I HDAC inhibitors, we screened compounds **1a-1l** against HEK293 cell lysates using a fluorogenic acetylated lysine substrate. All compounds were tested thrice against HEK293 lysate and recombinant HDAC3. If the compound was found to possess an IC_{50} less than 100 nM against HDAC3 and less than 1000 nM against HEK293 lysate, it was tested thrice against recombinant HDACs 1 and 2 to determine selectivity for class I. The summation of the corresponding findings are summarized in **Table 1**, with data for HDACs 1 and 2 in **Supporting Information Table S1**.

The relatively inefficacious compounds **1b**, **1d**, **1f**, and **1g** demonstrated that heterocyclic substitution was not favored compared to phenyl groups. Further, a para position oxygen provided mild benefit as seen in compounds **1a** and **1c**. However, a carbon, whether aliphatic or aromatic, was superior in this position, as seen in **1e** and **1l**. Interestingly, the creation of an unsaturated bond at the alpha position to the carbonyl, as seen in compound **1i,** provided ~6-fold increased HDAC3 inhibition when compared to its saturated counterpart **1h**. This can be explained as it creates an acrylamide-like structure which is likely capable of forming covalent bonds with cysteine residues on the HDAC enzyme; allowing for enhanced inhibition ability. While neither compound was particularly potent, it was interesting to see the sharp difference in activity between **1j** and **1k**. This possibly demonstrates that the binding pocket near this position is relatively narrow and the wider surface area of the 1-naphthyl group of **1j** is unable to bind adequately, whereas the 2-naphthyl group of **1k** is able to fit more reasonably or is less sterically hindered. The compound **1l** possessed the most potent carbonyl attachment, with an IC_{50} of less than 10 nM and K_i of less than 2 nM for HDAC3 and 8- to 10-fold selectivity for HDAC3

compared to HDACs 1 and 2. Using this finding, we next pursued structure activity relationships on substitutions of the β-nitrogen relative to the hydrazide.

Chemistry of N-(4-(hydrazide)benzyl)benzamide analogs. We began our second refinement synthetic scheme by generating the N-(4-(hydrazinecarbonyl)benzyl)benzamide which would be used in all subsequent reactions for this group. This was achieved as shown in **Scheme 2**, reactions a-c. Briefly, the starting material, 4-(aminomethyl)benzoic acid, was refluxed in methanol and concentrated acid to generate the much more soluble corresponding methyl ester hydrochloride salt (**Scheme 2**, reaction a). This intermediate was reacted with benzoyl chloride in ethyl acetate and water in the presence of potassium carbonate to form an amide bond and afford 4-(benzamidomethyl)benzoate (**Scheme 2**, reaction b). This was in turn refluxed with the hydrazine water salt in methanol to generate the desired intermediate (**Scheme 2**, reaction c). Lastly, this intermediate was N-methylated using various aldehydes in ethanol and magnesium sulfate followed by reduction using sodium cyanoborohydride in acidified methanol to yield the desired products, **2a**-**2m** (**Scheme 2**, reactions d and e).

HDAC inhibition of series 2 inhibitors. We screened compounds **2a**-**2m** thrice against HEK293 lysates and recombinant human HDAC3; the resulting data is summarized in **Table 2**. Compounds demonstrating an IC_{50} less than 100 nM against HDAC3 and less than 1000 nM against HEK293 lysates were then tested thrice against recombinant HDACs 1 and 2 to determine selectivity profiles. Data from HDACs 1 and 2 can be found in **Supporting Information Table S2**. Generally, branched alkyl substitution, as seen in **2b**, provided inferior inhibition compared to non-branched analogs such as **2d**. There was an overall decrease in

inhibition as the chain length increased past six carbons seen with compounds **2h, 2i,** and **2k**. Cyclic additions at the end of alkyl chains, such as those seen in **2g** and **2m**, provided negligible effects. Lastly, the addition of a trifluoro group for compound **2f** provided worse HDAC3 inhibition compared to the non-fluorinated **2d**. Overall, very little potency was gained from this refinement series, seeing the slight benefit of an N-substituted propyl chain of **2d** compared to the corresponding butyl chain of **1l** which dropped the IC_{50} to less than 5 nM and lowered the K_i to the sub-nanomolar range for HDAC3.

Chemistry N-(4-(hydrazide)benzyl)cinnamamide analogs. With the information from our second structure-activity relationship study providing insight that a non-branched propyl chain substitution on the β-nitrogen of the hydrazide seemingly is ideal, we moved forward by further modifying the carbonyl substituent. We noticed an increase in the use of N-hydroxylated acrylamide groups for HDAC inhibitors, present even in panobinostat and belinostat, as well as a multitude of pre-clinical inhibitors. This motif is a known Michael acceptor and likely forms covalent bonds with the sulfhydryl group of cysteines on proteins in vivo. Curious to see the effect on efficacy of incorporating an α, β unsaturated ketone, a similar Michael acceptor, we developed a cinnamamide derivative to build off of. This was achieved by again refluxing 4-(aminomethyl)benzoic acid in acidified methanol (**Scheme 3**, reaction a). Cinnamoyl chloride was formed using cinnamic acid and performing an acyl chlorination using oxalyl chloride in methylene chloride with catalytic amounts of dimethylformamide (**Scheme 3**, reaction b). The product of this reaction was mixed with the benzoate from reaction a in a 1:1 (v/v) mixture of ethyl acetate and water with potassium carbonate to form the corresponding amide bond (**Scheme 3**, reaction c). Here, we reacted this compound with lithium hydroxide in a solution of

methanol, water, and tetrahydrofuran (2:1:2 v/v) to generate the corresponding carboxylic acid (**Scheme 3**, reaction d). While it was never attempted, reactions c and d may theoretically be combined using lithium hydroxide in place of potassium carbonate in reaction c to cleave the methyl ester while also simultaneously forming the amide bond. With the carboxylic acid generated, we performed an amine coupling with HOBt and DCC in dimethylformamide (**Scheme 3**, reaction e). This intermediate was then reacted with a hydrazine water salt at 0°C. Finally, the hydrazide was reacted with the aldehyde of interest in ethanol with addition of magnesium sulfate and subsequently reduced using sodium cyanoborohydride in acidified methanol to yield compounds **3a**-**3e** (**Scheme 3**, reactions f and g).

HDAC inhibition of series 3 inhibitors. We ended our in vitro screening by interrogating the IC_{50} values of **3a**-**3e** against HEK293 lysates and recombinant human HDACs 1, 2, and 3. The results from these studies are listed in **Table 3**. The most striking change when comparing this cinnamamide derivative to the benzamide derivatives are their potencies. All compounds tested display less than 40 nM IC_{50} values against HDAC3 with the exception of the hexyl chain containing **3e**. The lead candidate from this study was the propyl chain containing **3b**, possessing a sub-nanomolar IC_{50} and K_i against HDAC3 with 10- and 100-fold selectivity toward HDACs 1 and 2, respectively. The butyl chain derivative, **3c**, that mimicked the substituent of the very potent **1l** provided single-digit nanomolar potency against HDAC3, yet was approximately 3-5 fold weaker when compared to **3b**. These findings suggest that a β-nitrogen alkyl substituent chain length of 3-4 carbons provides ideal conditions, with the ethyl, pentyl, and hexyl groups of **3a**, **3d**, and **3e,** respectively, having diminished inhibitory prowess when compared to **3b** or **3c**.

Mass spectrometric analysis of select hydrazide-based inhibitors in glucuronidating environments. To demonstrate that these compounds were indeed highly unlikely to be glucuronidated in vivo, we adapted and performed an ex vivo assay using a protocol derived from Walsky and colleagues.[44] Briefly, vorinostat, **1l**, **2d**, and **3b** were incubated with human liver microsomes, UDP Glucuronic acid, and alamethicin (a pore-forming antibiotic) for 12 hours at 37°C. The reaction was quenched with a 47:50:3 (v/v) mixture of water:acetonitrile:formic acid. The vessel was subjected to centrifugation and the supernatant filtered and examined via electrospray ionization liquid chromatography mass spectrometry. A parallel study that lacked UDP Glucuronic acid was performed with each inhibitor as a negative control. Comparing **Figure 1a** (blue) and **Figure 1b** (red) demonstrates the presence of the *o*-glucuronidated metabolite of vorinostat with a $(m+H^+)/z$ of 441.04 (**Figure 1b**, bottom right), in line with previous findings.[45] This mass shift was not present in the corresponding negative control lacking UDP Glucuronic acid (**Figure 1a**, middle right). There are no differences between masses or ionization patterns in any of the hydrazide-containing compounds (**Figures 1c-d**, **Supporting Information Figures S1a-d**), suggesting these compounds are not readily glucuronidated in environments where vorinostat is extensively glucuronidated. It was also noted that **3b**, possessing an unsaturated bond, was reduced in this model, despite no NADPH being added to the reaction vessel (**Supporting Information Figures S1c-d**). This may demonstrate a potential metabolite of this compound.

Interrogation of in vitro binding kinetics of hydrazide-containing HDAC inhibitors. Generally speaking, the very reason why groups like *ortho*-aminoanilide or hydroxamates are

able to chelate zinc and other dicationic metals is the same reason why they are prime glucuonidation targets. Their possession of primary alcohols and primary amines not only allow them to ionically complex with the positively charged zinc, but also allows them to be extensively inactivated via glucuronidation. After demonstrating that the hydrazide motif was not glucuronidated in ex vivo environments, we questioned whether it was inhibiting HDACs through a direct active zinc chelation. We hypothesized that the compound should demonstrate typical Michaelis-Menten competitive inhibition, similar to vorinostat, if it was truly chelating zinc in the active site of HDACs. Thus, we performed in vitro V_{max} studies using recombinant HDACs 1 and 3 and compounds **2d** and **3b**. Applying a double reciprocal conversion of the data yielded Lineweaver-Burke plots. Surprisingly, and contrary to previous data, our hydrazide-containing compounds clearly demonstrate a convergence in the 2nd quadrant, indicative of mixed inhibition (**Figures 2a-b**) and non-competitive inhibition (**Figures 2c-d**). This is in direct contrast to the initial findings published by Wang and colleagues.[42] Their published data seem to match a canonical competitive inhibitor, with their corresponding Lineweaver-Burke plots demonstrating all doses and control intersecting directly on the y-axis, representative of $1/V_{max}$. However, the corresponding V_{max} plots from which these graphs were derived display changes in V_{max}. This would mean the y-intercepts on the double reciprocal Lineweaver-Burke plots should be different as well. To further ensure our findings were valid, we used vorinostat as a positive control, a known competitive inhibitor with extensive kinetic analyses published independently.[46] Matching established data, our results demonstrated complete convergence directly on the y-axis, indicative of competitive inhibition (**Figures 2e-f**), which is in direct agreement with the very similar V_{max} values seen at each dose. This finding, coupled with the lack of glucuronidation ex vivo, points to an allosteric binding site on class I HDACs that is

strongly inhibited by our hydrazide-containing inhibitors, and has little to do with catalytic site zinc chelation. The V_{max} plots from which these Lineweaver-Burke plots were derived may be seen in **Supporting Information Figures S2a-f**.

HDAC3 molecular docking study of HDAC inhibitors. With the results thus far suggesting an allosteric binding site, we were curious if we could identify a potential site at which our inhibitors were binding. Using the solution structure of HDAC3 bound to Ncor2, pdb: 4A69, we probed the HDAC3 surface with **3b** resulting in a heavy concentration of poses near the interface with the Ncor2 coenzyme (**Supporting Information Figure S3a**). We then calculated the propensity for ligand interaction which revealed a very positive binding region directly overlapping with the high density **3b** binding area (**Supporting Information Figure S3b**). Using this pocket, we performed a flexible induced fit binding of **2d**, **3b**, and vorinostat and calculated binding scores from the top 20 (lowest energy) poses from each set. Our lead inhibitors **2d** and **3b** display nearly identical binding scores, which is line with their near identical in vitro activity and electrospatial occupancies. The canonical binder vorinostat bound less tightly to this pocket, as evidenced by its higher energy posing scores (**Supporting Information Figure S3c**). Lastly, when we posed the lowest energy poses for 2d and 3b, we see significant overlap in electrospatial occupancy, indicative of homologous modes of binding (**Figure 3a**), whereas the lowest pose for vorinostat results in a completely different orientation, with the hydroxamic acid exposed to solvent and its phenyl group serving as the main area of interaction (**Figure 3b**). Additionally, a narrow tunnel can be seen where the propyl hydrazide of both **2d** and **3b** fit nicely. This matches the in vitro and ex vivo data demonstrating that adding branching alkyl chains, or extending the alkyl chains past a length of four carbons leads to

markedly diminished inhibition activity. Taken together, these findings illustrate the potential for a novel, allosteric binding site that the propyl hydrazide motif is particularly astute at fitting into.

Efficacy of lead analog in ex vivo cell models. Satisfied with results of our three structure activity studies and the potential for allosteric inhibitors that are impervious to glucuronidation, we transitioned from recombinant enzyme pre-screening to cellular treatment. Given that HDAC inhibitors are most successful in hematologic malignancies such as lymphomas and myelomas, as shown by their FDA approvals, we screened our most potent inhibitor, **3b**, against an array of leukemia and Multiple Myeloma cell lines. Briefly, Molm-14, an acute monocytic leukemia cell line[47]; HL-60, an acute promyelocitic cell line[48]; RS4-11, an acute lymphoblastic leukemia[49]; K562, a chronic myelogenous leukemia[50]; MV4-11, an acute myeloid leukemia[51]; and RPMI-8226, a Multiple Myeloma cell line[52], were all used to determine the efficacy of **3b** against a multitude of different hematologic cancers. Cells were treated for 48 hours before viability was assessed with CellTiter-Blue Cell Viability Assay. The active fluorescent reagent in this assay is resazurin. This molecule is converted by the functional mitochondria in the viable cells to resorufin. Resorufin intensity is therefore directly related to cell viability. The resulting EC_{50} values from each cell line is summarized in **Table 4**. **3b** demonstrates the highest level of potency against the AML cell line MV4-11; possessing an EC_{50} for the cells at less than 50 nM. Taken together with the efficacy toward Molm14 and RS4-11, both acute myeloid leukemia subsets, we can see that **3b** is particularly selective for acute types of leukemia when compared to its lack of efficacy toward the chronic leukemia cell line, K562 or the chromosomal translocation containing HL-60 cell line. Further, when tested against the classical Multiple Myeloma cell line, RPMI-8226, **3b** demonstrated incomplete kill curves even at mM

concentrations. Following the potency findings of **3b** in MV4-11 cells, we assessed the efficacy of **1l**, **2d**, and **3b** in these cells as single agents. Panobinostat, vorinostat, entinostat, **1l**, **2d**, and **3b** were tested against MV4-11 for 48 hours of treatment. Cells were treated with CellTiter-Blue to determine viability which was measured using a spectrophotometer as a function of resorufin intensity. Results from these experiments are shown as an EC_{50} cell viability curve in **Figure 4a**. As a negative control, we also performed this experiment using **2c**, a compound whose structure very closely matches **2d**, differing only by a non-reduced nitrogen-carbon bond, while possessing no appreciable inhibition against recombinant HDAC3. Matching its weak prowess as an HDAC inhibitor from our recombinant HDAC assay, this compound demonstrated no appreciable activity against MV4-11 cells even at doses as high as 250 μM (**Supporting Information Figure S4a)**.

As single agents, these compounds possess less than 300 nM EC_{50} values against MV4-11 with complete kill curves. To demonstrate that our initial HDAC activity pre-screening assay was correlative with efficacy against MV4-11 cells, we plotted the compounds' respective potency toward HEK293 lysates as a function of their IC_{50} with their respective EC_{50} values against MV4-11 cells (**Supporting Information Figure S4b**). The results demonstrate a linear relationship with considerable correlation, demonstrating the ability of our HDAC activity pre-screen assay to translate to ex vivo potency in AML cells.

To further demonstrate the correlation between MV4-11 cell death with hyperacetylation of histones H3 and H4, we performed Western blot analysis of MV4-11 cell lysates after 24 hour treatment with 100 nM of inhibitor (**Figure 4b**). The data demonstrate that our lead inhibitors, **1l**, **2d**, and **3b** are more potent at increasing the concentrations of acetylated histones H3 and H4, markers of HDACs 1, 2, and 3 inhibition, than the FDA approved vorinostat or the *ortho*-

aminoanilide-based entinostat (**Figure 4b-c**). Additionally, this upregulation is dose-dependent, with increasing levels of hyperacetylation seen with increasing concentrations of inhibitor (**Figure 4d**). As a negative control, we once again used **2c** to further ensure the validity of our pre-cellular screening. At a concentration of 100 nM, **2c** was also used in MV4-11 cells for western blot analysis and demonstrated no appreciable ability to increase acetylation of histones H3 and H4 (**Supporting Information Figure S4c).** Further, upregulation of histones H3 and H4 is selective, as our hydrazide based inhibitors do not demonstrate any effect on levels of acetylated tubulin, a marker of HDAC6 inhibition (**Figures 4b** and **3d**). This is an important characteristic, as upregulation of acetylated histones H3 and H4 is inversely and logarithmically correlated with EC_{50} against AML, that is, an increase in acetylated histones H3 and H4 leads to an exponential decrease in EC_{50} against these cells (**Supporting Information Figures S4d-e**). This is in sharp contrast to acetylated tubulin, where increasing levels of acetylation are not as directly correlative with EC_{50} against MV4-11 cells (**Figure 4b**).

Selectivity and toxicity profiling of lead analogs. Concluding our experiments, we sought to determine if the hydrazide based inhibition of HDACs was a non-selective cell death mechanism, or if it was selective toward non-solid tumor cells, particularly various forms of leukemia. We examined the ex vivo effect of **1l**, **2d**, and **3b** in HEK293 and HeLa cells, well-studied solid tumor cell lines. Briefly, cells were pre-incubated for 24 hours prior to treatment. After treatment, cells were incubated for an additional 48 hours before measurement of cell viability as a function of resorufin intensity was determined. The corresponding EC_{50} values demonstrate at least 100 fold higher selectivity toward the MV4-11 cell line (compare **Figures 4a** and **5a-b**). Further, we wanted to examine our lead compounds' toxicity profile against healthy human

peripheral blood mononuclear cells (PBMCs). PBMCs were treated with titrating doses of panobinostat, **2d**, or **3b** for 24 hours followed by treatment with CellTiter-Blue. Cell viability was determined as a function of resorufin intensity via spectrophotometer, normalized to control treatment. The data demonstrate **2d** and **3b**'s superiority over panobinostat from a toxicity standpoint. Further, the lack of a Michael acceptor group on **2d** seems to reduce its toxicity toward PBMC's 10 fold compared to **3b** (**Figure 5b**). This functional group (present as an acrylamide) may also explain panobinostat's much greater toxicity compared to **2d** and **3b**.

DISCUSSION

To date, all FDA approved HDAC inhibitors or those in clinical trials contain promiscuous metal-chelating groups. The hydroxamic acid was the first metal-chelating group to be introduced, and to this day remains the most common, but others such as the disulfide bond of romidepsin, or the *ortho*-aminoanilide of entinostat have also been used. These groups are all generally acidic in nature, and have been shown to be subject to glucuronidation. This addition of steric bulk and charge neutralization removes the ability of these inhibitors to get into the narrow active site and ionically bind to the positively charged zinc that is paramount to HDAC deacylase activity. In this study we demonstrated that very potent and selective inhibition of class I HDACs is possible with the novel utilization of the metal chelating group, hydrazide. Further, we demonstrated that these compounds likely work through an allosteric mode of inhibition. This possibly indicates the presence of a non-catalytic metal-center target of these hydrazide compounds. Thus far, discoveries of allosteric, small molecule inhibitors of class I HDACs have not been well established in the literature. Inhibitors that lack a known metal-

chelating group that have been shown to inhibit HDACs were shown to display canonical competitive Michaelis-Menten enzyme kinetics when further interrogated.[53]

The results in this manuscript suggest our compounds are also highly resistant to glucuronidation, indicating they possess little anionic charge, and display mixed/non-competitive inhibition, giving further credibility to the possibility that they may bind to a non-catalytic site on HDACs irrespective of whether substrate is bound. Further, this allosteric site is present ex vivo, as their recombinant enzyme inhibition prowess translated directly to cellular efficacy as well. Discovery of a potential allosteric binding site benefits more than just medicinal chemistry surrounding HDAC inhibitors. By having a combination of agents that work both at the active site, and allosterically on HDACs, the possibility of dual mechanism therapies for acute myeloid leukemia arises.

Lastly, while this paper established a >60 fold improvement in potency over the initial lead inhibitor generated by Wang and colleagues, our most potent of which breaching the picomolar range for recombinant human HDAC3 inhibition, further refinement of these inhibitors is also possible. Further alterations surrounding N-benzylbenzamide group that provided so much of these molecules' potencies would be the first place to start. Stepwise methylation at key sites, or the introduction of electron donating or withdrawing groups around either of the phenyl rings could provide additional potency.

Our lead inhibitors **1l**, **2d**, and **3b**, were used ubiquitously throughout the manuscript. All of these agents display higher levels of ex vivo potency than vorinostat or entinostat. The most potent, **3b**, contains a Michael-acceptor group in the form of an α, β-unsaturated ketone. While once a forbidden group in medicinal chemistry, recently approved effective therapies such as dimethyl fumarate demonstrate that not all Michael-acceptors are detrimental to patient health,

even in long term use. However, when comparing **3b**'s potency to that of **2d**, we see an approximate 2.5 fold decrease in EC_{50} in MV4-11 cells at the cost of a 10 fold increase in PBMC based toxicity. Further, this was the only one of our compounds tested in human liver microsomes to demonstrate a metabolite, being reduced about its unsaturated bond. This was surprising, as no external reducing substrates such as NADH or NADPH were added to the reaction vessel. This indicates that even the residual concentrations of these reducing agents leftover from extraction were enough to metabolize this compound. As such, the superior metabolic stability, and better toxicity profiles of **2d** make it a more beneficial candidate worth pursuing.

EXPERIMENTAL PROCEDURES

General Chemistry. All reagents and chemical solvents were used from the respective commercially available sources without further purification. ^{1}H NMR and ^{13}C NMR data were collected in deuterated solvent with a Bruker 400 MHz with Trimethylsilane as a standard reference. Chemical shifts are given in parts per million. NMR descriptions use the following abbreviations: s = singlet, d = doublet, t = triplet, q = quartet, m = multiplet, and br = broad peak. Coupling constants (*J*) reported in Hz. Mass spectra data were gathered using a Thermo LCQ Fleet mass spectrometer using electrospray ionization. Purification was performed using a Teledyne Isco Combiflash 200 on prepacked C18 columns. All target compounds were at least 95% pure confirmed via UV detection (λ = 254 nm) on a Thermo LCQ Fleet HPLC-MS using an Accucore RP-MS HPLC Column, 2.6 μm particle size, 30x4.6 mm. These runs used water and methanol with 0.1% (v/v) formic acid were used as mobile phase. A gradient of 100% water was run isocratically for 0.5 minutes at 500 μL/min. The gradient then increased to 100% methanol

over 13.5 minutes, and run isocratically for one minute before returning to 100% water over the next two minutes. Capillary temperature was 350°C, with a spray voltage of 5 kV. Purity was calculated using the automatic peak detection function followed by dividing the area under the curve of the peak by the total area of all peaks in the chromatograph.

Figure Creation. Figures were generated using Adobe Illustrator CC, Adobe Photoshop CC, Image Studio Lite 4.0, GraphPad Prism 6.0, ChemDraw 13.0, and Microsoft PowerPoint 2013.

Synthesis of butylhydrazide derivatives (1a-1l).

Series 1 General Procedure. Once the corresponding hydrazide was generated, 1.1 equivalents of butaldehyde and 10 equivalents of magnesium sulfate were stirred in 10 mL of ethanol with the hydrazide. The reaction was stirred at room temperature and monitored via TLC. After disappearance of starting material, the excess magnesium sulfate was removed via vacuum filtration, and the collected solution condensed under vacuum. The intermediate was resuspended in 4 mL of methanol followed by addition of 1.2 equivalents of sodium cyanoborohydride and a pinch of methyl orange. Argon was bubbled through the resulting yellow solution for 5 minutes. At this time a solution of concentrated HCl in methanol (1:1 v/v) was added dropwise until the solution turned and stayed red. The mixture was allowed to stir overnight under argon. Volatiles were removed under vacuum and purified on C18 reverse phase columns eluted with acetonitrile and water to yield the desired product.

N'-butyl-4-methoxybenzohydrazide (**1a**). 498.54 mg (3 mmol) of 4-methoxybenzohydrazide was reacted as described in **Series 1 General Procedure** to yield 317.9 mg of dry product (48% yield). ^{1}H NMR (400 MHz, DMSO): δ 9.89 (s, 1H), 7.82 (d, J = 8.8 Hz, 2H), 6.99 (d, J = 8.8 Hz,

2H), 4.99 (s, 1H), 3.81 (s, 3H), 2.79-2.76 (m, 2H), 1.48-1.40 (m, 2H), 1.38-1.32 (m, 2H), 0.89 (t, J = 7.2 Hz, 3H). ^{13}C NMR (100 MHz, DMSO): δ 165.4, 162.0, 129.3, 125.9, 114.0, 55.8, 51.5, 30.3, 20.3, 14.3. [(m+H$^+$)/z = 223.25]. (λ_{254}) purity 95.4%, t_R 9.28 mins.

N'-butylbenzofuran-2-carbohydrazide (**1b**). 324.0 mg (2 mmol) of benzofuran-2-carboxylic acid was suspended in 5 mL of methylene chloride. The flask was flushed with argon for 10 minutes before injection of 0.4 mL (4 mmol) oxalyl chloride. Two drops of dimethylformamide were injected and furious bubbling began. The sealed vessel was continuously flushed with argon and vented for 2 hours at room temperature. 10 mL of sieve dried ethanol was slowly injected and allowed to stir for an additional hour. Volatiles were removed under vacuum and the crude intermediate was resuspended in 5 mL ethanol. To this solution was added 250 mg (5 mmol) of hydrazine water salt. The reaction was refluxed for 3 hours to give the corresponding hydrazide. Volatiles were removed under vacuum and the product suspended in 10 mL of ethanol. From here the reaction proceeded as described in **Series 1 General Procedure** to yield 369.1 mg of dry product (72% yield). ^{1}H NMR (400 MHz, DMSO): δ 10.26 (d, J = 6.0 Hz, 1H), 7.78 (d, J = 8.0 Hz, 1H), 7.66 (d, J = 8.4 Hz, 1H), 7.54 (s, 1H), 7.49-7.45 (m, 1H), 7.36-7.32 (m, 1H), 5.16-5.13 (m, 1H), 2.84-2.79 (m, 2H), 1.48-1.41 (m, 2H), 1.39-1.33 (m, 2H), 0.90 (t, J = 7.2 Hz, 3H); ^{13}C NMR (100 MHz, DMSO): δ 157.7, 154.7, 148.7, 127.5, 127.2, 124.2, 123.1, 112.2, 109.6, 51.2, 30.2, 20.3, 14.4. [(m+H$^+$)/z = 233.25]. (λ_{254}) purity 98.8%, t_R 11.53 mins.

N'-butyl-4-phenoxybenzohydrazide (**1c**). 685 mg (3 mmol) of 4-phenoxybenzohydrazide was suspended in 10 mL of ethanol. From here the reaction proceeded as described in **Series 1 General Procedure** to yield 596.7 mg of dry product (70% yield). ^{1}H NMR (400 MHz, DMSO): δ 9.99 (s, 1H), 7.88 (d, J = 8.8 Hz, 2H), 7.46-7.42 (m, 2H), 7.23-7.20 (m, 1H), 7.09 (d, J = 8.0 Hz, 2H), 7.03 (d, J = 8.8 Hz, 2H), 5.07 (s, 1H), 2.81-2.77 (m, 2H), 1.47-1.41 (m, 2H), 1.38-1.32

(m, 2H), 0.89 (t, J = 7.2 Hz, 3H); ^{13}C NMR (100 MHz, DMSO): δ 165.1, 159.9, 156.1, 130.7, 129.7, 128.4, 124.7, 119.9, 117.9, 51.4, 30.3, 20.3, 14.4. [(m+H$^+$)/z = 285.25]. (λ_{254}) purity 98.2%, t_R 12.60 mins.

N'-butylnicotinohydrazide (**1d**). 1068 mg (6 mmol) of nicotinoyl chloride was suspended in 20 mL of methanol. To this solution was added 1.7 mL (12 mmol) of triethylamine. The reaction was stirred at room temperature for 1 hour. 750 mg (15 mmol) hydrazine water salt was added and the solution was refluxed for 3 hours yielding the corresponding hydrazide. Volatiles were removed under vacuum and the intermediate was resuspended in 30 mL of methanol. From here the reaction proceeded as described in **Series 1 General Procedure** to yield 721.7 mg of dry product (62% yield). ^{1}H NMR (400 MHz, DMSO): δ 10.21 (s, 1H), 8.99 (s, 1H), 8.72-8.70 (m, 1H), 8.19-8.10 (m, 1H), 7.52-7.49 (m, 1H), 5.15 (s, 1H), 2.83-2.79 (m, 2H), 1.48-1.42 (m, 2H), 1.38-1.32 (m, 2H), 0.89 (t, J = 7.2 Hz, 3H); ^{13}C NMR (100 MHz, DMSO): δ 164.2, 152.3, 148.6, 135.2, 129.3, 124.0, 51.3, 30.2, 20.3, 14.4. [(m+H$^+$)/z = 194.25]. (λ_{254}) purity 95.6%, t_R 6.17 mins.

N'-butyl-[1,1'-biphenyl]-4-carbohydrazide (**1e**). 890 mg (3.8 mmol) of methyl [1,1']-biphenyl-4-carboxylate was suspended in 20 mL of methanol. To this solution, 945 mg (18.9 mmol) of hydrazine water salt was added. The solution was brought to reflux and reacted for 3 hours. The solution was cooled and volatiles evaporated under vacuum. From here the reaction proceeded as described in **Series 1 General Procedure** to yield 555.1 mg of dry product (54% yield). ^{1}H NMR (400 MHz, DMSO): δ 10.08 (d, J = 6 Hz, 1H), 7.94-7.92 (m, 2H), 7.78-7.73 (m, 4H), 7.52-7.48 (m, 2H), 7.44-7.40 (m, 1H), 5.13-5.09 (m, 1H), 2.84-2.79 (m, 2H), 1.49-1.42 (m, 2H), 1.40-1.35 (m, 2H), 0.91 (t, J = 7.2 Hz, 3H); ^{13}C NMR (100 MHz, DMSO): δ 165.4, 143.2, 139.6,

132.5, 129.5, 128.5, 128.2, 127.3, 127.0, 51.4, 30.3, 20.3, 14.4. [(m+H^+)/z = 269.25]. (λ_{254}) purity 96.7%, t_R 12.82 mins.

N'-butylthiophene-2-carbohydrazide (**1f**). 1500 mg (10 mmol) of thiophene-2-carbonyl chloride was injected into 10 mL of sieve dried methanol and bubbled with argon for 10 minutes. To this mixture was injected two drops of dimethylformamide. The reaction proceeded at room temperature for 1 hour before addition of 600 mg (12 mmol) hydrazine water salt. The solution was refluxed for 3 hours before being cooled and condensed in vacuo. The reaction then proceeded as described in **Series 1 General Procedure** to yield 1235 mg of dry product (62% yield). ^{1}H NMR (400 MHz, DMSO): δ 10.02 (s, 1H), 7.76-7.74 (m, 2H), 7.15-7.13 (m, 1H), 5.03 (s, 1H), 2.80-2.77 (m, 2H), 1.45-1.40 (m, 2H), 1.37-1.32 (m, 2H), 0.89 (m, J = 7.2 Hz, 3H); ^{13}C NMR (100 MHz, DMSO): δ 161.0, 138.8, 131.0, 128.4, 128.2, 51.3, 30.3, 20.3, 14.4. [(m+H^+)/z = 199.17]. (λ_{254}) purity 97.5%, t_R 8.47 mins.

N'-butylfuran-2-carbohydrazide (**1g**). 1100 mg (8.4 mmol) of furan-2-carbonyl chloride was injected into 10 mL of sieve dried methanol that was bubbled with argon for 10 minutes prior to addition. To this mixture was injected 1780 mg (17.6 mmol) of triethylamine. After 60 minutes, 1000 mg (20 mmol) of hydrazine water salt was added, and heated to reflux for 3 hours. The reaction was cooled and condensed under vacuum. From here the reaction proceeded as described in **Series 1 General Procedure** to yield 861 mg of dry product (56% yield). ^{1}H NMR (400 MHz, DMSO): δ 9.90 (s, 1H), 7.83-7.82 (m, 1), 7.11-7.10 (m, 1H), 6.62-6.60 (m, 1H), 5.00 (s, 1H), 2.79-2.74 (m, 2H), 1.44-1.40 (m, 2H), 1.38-1.30 (m, 2H), 0.88 (t, J = 7.2 Hz, 3H); ^{13}C NMR (100 MHz, DMSO): δ 157.6, 147.3, 145.4, 113.6, 112.1, 51.3, 30.2, 20.3, 14.4. [(m+H^+)/z = 183.17]. (λ_{254}) purity 98.4%, t_R 7.43 mins.

N'-butyl-3-phenylpropanehydrazide (**1h**). 1012 mg (6 mmol) of 3-phenylpropanoyl chloride was injected into 10 mL of argon bubbled, sieve dried methanol. The reaction was allowed to stir for 1 hour before addition of 900 mg (18 mmol) hydrazine water salt. The mixture was brought to reflux for 3 hours before being cooled to room temperature and condensed under vacuum. From here the reaction proceeded as described in **Series 1 General Procedure** to yield 911 mg of dry product (68% yield). ^{1}H NMR (400 MHz, DMSO): δ 9.25 (s, 1H), 7.29-7.25 (m, 2H), 7.21-7.26 (m, 3H), 4.77 (s, 1H), 2.82 (t, *J* = 7.6 Hz, 2H), 2.63-2.59 (m, 2H), 2.33 (t, *J* = 7.6 Hz, 2H), 1.31-1.25 (m, 4H), 0.85 (t, *J* = 7.2 Hz, 3H); ^{13}C NMR (100 MHz, DMSO): δ 170.5, 141.5, 128.7 (d), 126.3, 51.2, 35.6, 31.5, 30.1, 20.2, 14.4. [(m+H^{+})/z = 221.25]. (λ_{254}) purity 98.9%, t_R 8.56 mins.

N'-butylcinnamohydrazide (**1i**). 1480 mg (10 mmol) of trans-cinnamic acid was suspended in 50 mL of acetonitrile. To this solution was added 1620 mg (12 mmol) of 1-hydroxybenzotriazole and 2478 mg (12 mmol) N, N' –dicyclohexylcarbodiimide. The solution stirred overnight at room temperature before addition of 600 mg (12 mmol) hydrazine water salt, which was refluxed for 3 hours. The solution was brought to room temperature and condensed under vacuum. From here the reaction proceeded as described in **Series 1 General Procedure** to yield 885 mg of dry product (40% yield). ^{1}H NMR (400 MHz, DMSO): δ 9.62 (s, 1H), 7.58-7.56 (m, 2H), 7.45-7.38 (m, 4H), 6.57 (d, *J* = 16.0 Hz, 1H), 5.05 (s, 1H), 2.76-2.72 (m, 2H), 1.44-1.28 (m, 4H), 0.89 (t, *J* = 7.2 Hz, 3H); ^{13}C NMR (100 MHz, DMSO): δ 164.3, 139.0, 135.4, 129.9, 129.4, 127.9, 120.8, 51.4, 30.2, 20.2, 14.4. [(m+H^{+})/z = 219.25]. (λ_{254}) purity 97.5%, t_R 10.95 mins.

N'-butyl-1-napthohydrazide (**1j**). 1033 mg (6 mmol) of 1-napthoic acid was suspended in 20 mL of argon flushed methylene chloride. To this solution was injected 1143 mg (9 mmol) of oxalyl chloride followed by injection of 2 drops of dimethylformamide. Furious bubbling was seen, with gas being exhausted and argon flushing continually throughout the room temperature

reaction. After one hour, 20 mL of sieve dried methanol was injected slowly. After reacting for an additional hour at room temperature, the solution was condensed under vacuum and resuspended in 30 mL of methanol. To this was added 1500 mg (30 mmol) of hydrazine water salt. The reaction was brought to reflux for 3 hours before being cooled and condensed under vacuum. From here the reaction proceeded as described in **Series 1 General Procedure** to yield 1050 mg of dry product (72% yield). ^{1}H NMR (400 MHz, DMSO): δ 9.97 (s, 1H), 8.22-8.19 (m, 1H), 8.04-7.98 (m, 2H), 7.61-7.53 (m, 4H), 5.23 (s, 1H), 2.92-2.87 (m, 2H), 1.53-1.42 (m, 2H), 1.40-1.38 (m, 2H), 0.93 (t, J = 7.2 Hz, 3H); ^{13}C NMR (100 MHz, DMSO): δ 167.8, 133.7, 133.6, 130.4, 130.4, 128.7, 127.2, 126.7, 125.8, 125.7, 125.5, 51.3, 30.3, 20.3, 14.4. [(m+H^{+})/z = 243.25]. (λ_{254}) purity >99%, t_R 11.00 mins.

N'-butyl-2-napthohydrazide (**1k**). 1120 mg (6 mmol) of 2-napthohydrazide was reacted as described in **Series 1 General Procedure** to yield 1016 mg of dry product (70% yield). ^{1}H NMR (400 MHz, DMSO): δ 10.2 (s, 1H), 8.46 (s, 1H), 8.04 -7.93 (m, 4H), 7.64-7.58 (m, 2H), 5.17 (s, 1H), 2.87-2.83 (m, 2H), 1.51-1.46 (m, 2H), 1.41-1.35 (m, 2H), 0.91 (t, J = 7.2 Hz, 3H); ^{13}C NMR (100 MHz, DMSO): δ 165.8, 134.6, 132.6, 131.1, 129.3, 128.4, 128.1, 128.0, 127.8, 127.2, 124.4, 51.4, 30.3, 20.3, 14.4. [(m+H^{+})/z = 243.25]. (λ_{254}) purity >99%, t_R 11.42 mins.

N-(4-(2-butylhydrazine-1-carbonyl)benzyl)benzamide (**1l**). To a mixture of sieve dried methylene chloride, was added 711 mg (4 mmol) of methyl 4-(aminoethyl)benzoate. This vessel was flushed with argon for 30 minutes before injection of 560 mg (4 mmol) of benzoyl chloride and 607 mg (6 mmol) of trimethylamine. The reaction was stirred at room temperature for 2 hours before being condensed under vacuum. The crude intermediate was resuspended in 30 mL of methanol and 1000 mg (20 mmol) of hydrazine water salt was added as one portion. The solution was refluxed for 3 hours before being cooled and condensed under vacuum. From here

the reaction proceeded as described in **Series 1 General Procedure** to yield 601 mg of dry product (46% yield). ^{1}H NMR (400 MHz, DMSO): δ 9.99 (s, 1H), 9.13-9.10 (t, J = 6.0 Hz, 1H), 7.93-7.91 (m, 2H), 7.81-7.79 (m, 2H), 7.57-7.47 (m, 3H), 7.41-7.39 (m, 2H), 5.07 (s, 1H), 4.54 (d, J = 6.0 Hz, 2H); ^{13}C NMR (100 MHz, DMSO): δ 166.7, 165.6, 143.5, 134.7, 132.2, 131.8, 128.8, 12.7, 127.6, 127.5, 51.4, 42.9, 30.3, 20.3, 14.4. HRMS-ESI [(m+H^{+})/z] calculated for $C_{19}H_{23}N_3O_2$: 326.18697; found, 326.18622. (λ_{254}) purity 96.3%, t_R 11.92 mins.

Synthesis of N-(4-(hydrazide)benzyl)benzamide derivatives (2a-2m).

Intermediate formation. 6050 mg (40 mmol) of 4-(aminomethyl)benzoic acid was dissolved in 200 mL of methanol, to which was added 6 mL of concentrated HCl in one portion. The mixture was refluxed overnight and the volatiles condensed under vacuum. The resulting white solid was suspended in ethyl ether and separated via vacuum filtration to yield the benzoate HCl salt. This compound was dissolved in a 1:2 mixture of ethyl acetate and water and chilled to 0°C to which 11040 mg (80 mmol) was added followed by addition of 5623 mg benzoyl chloride (40 mmol). The vessel was warmed to room temperature and stirred for 2 additional hours. The mixture was separated via acid/base extraction, washing the water phase twice with ethyl acetate. All organic phases were combined and condensed under vacuum to yield a white solid. This was suspended in 200 mL of methanol and 10000 mg (200 mmol) of hydrazine water salt was added. The solution was refluxed for 48 hours, cooled to room temperature, and volatiles were removed under vacuum. This intermediate (**2sm**) was used as the starting material for all further reactions for this family.

Series 2 General Procedure. The mixture of **2sm** and aldehyde of interest were stirred at room temperature overnight; vacuum filtration afforded the desired intermediate, which was dissolved

in 30 mL of methanol. To this solution was added a pinch of methyl orange, and the solution's color turned yellow. The solution was bubbled under argon for 5 minutes, and 2.2 mmol of sodium cyanoborohydride was then added to it. A 1:1 mixture of methanol and concentrated HCl was added dropwise until the solution turned red. After addition, the mixture was stirred at room temperature for 6 hours. The reaction was quenched with sodium hydroxide, and organic solvents were removed under vacuum. The residues were extracted twice with ethyl acetate, and organic phases were combined and dried over magnesium sulfate. After filtration, organic solvents were removed and the residues were purified by flash chromatography.

(E)-N-(4-(2-(but-2-en-1-yl)hydrazine-1-carbonyl)benzyl)benzamide (**2a**). 2 mmol of **2sm** was dissolved in 100 mL ethanol with ultra-sonication aid. To this solution was added 40 mmol of magnesium sulfate and 2 mmol of (E)-but-2-enal. From here the reaction proceeded as described in **Series 2 General Procedure** to yield 208 mg (32% yield). ^{1}H NMR (400 MHz, DMSO): δ 9.97 (d, *J* = 5.6 Hz, 1H), 9.12 (t, *J* = 6.0 Hz, 1H), 7.93-7.91 (m, 2H), 7.81-7.78 (m, 2H), 7.58-7.48 (m, 3H), 7.41-7.39 (m, 2H), 5.63-5.50 (m, 2H), 5.11-5.07 (m, 1H), 4.54 (d, *J* = 6.0 Hz, 2H), 3.37-3.35 (m, 2H), 1.65 (d, *J* = 5.6 Hz, 3H); ^{13}C NMR (100 MHz, DMSO): δ 166.8, 165.7, 143.5, 134.7, 132.2, 131.8, 128.8, 128.4, 128.2, 127.7, 127.6, 127.5, 53.6, 42.9, 18.2. [$(m+H^{+})/z$ = 324.17]. (λ_{254}) purity >99%, t_R 10.00 mins.

N-(4-(2-isopropylhydrazine-1-carbonyl)benzyl)benzamide (**2b**). 2 mmol of **2sm** was dissolved in 100 mL ethanol with ultra-sonication aid. To this solution was added 40 mmol of magnesium sulfate and 2 mmol of isopropanal. From here the reaction proceeded as described in **Series 2 General Procedure** to yield yielded 324 mg (52% yield). ^{1}H NMR (400 MHz, DMSO): δ 9.95 (d, *J* = 6.8 Hz, 1H), 9.11 (t, *J* = 6.0 Hz, 1H), 7.92-7.90 (m, 2H), 7.82-7.80 (m, 2H), 7.58-7.48 (m, 3H), 7.41-7.39 (m, 2H), 4.95-4.92 (m, 1H), 4.53 (d, *J* = 6.0 Hz, 2H), 3.11-3.03 (m, 1H), 1.02 (d,

J = 10.4 Hz, 6H); ^{13}C NMR (100 MHz, DMSO): δ 166.8, 166.0, 143.5, 134.7, 132.2, 131.8, 128.8, 127.7, 127.6, 127.4, 50.8, 42.9, 21.4. [(m+H$^+$)/z = 312.25]. (λ_{254}) purity 98.8%, t_R 8.68 mins.

(E)-N-(4-(2-propylidenehydrazine-1-carbonyl)benzyl)benzamide (**2c**). 2 mmol of **2sm** was dissolved in 100 mL ethanol with ultra-sonication aid. To this solution was added 40 mmol of magnesium sulfate and 2 mmol of propanal. From here the reaction proceeded as described in **Series 2 General Procedure** to yield 347 mg (56% yield). ^{1}H NMR (400 MHz, DMSO): δ 11.39 (s, 1H), 9.13 (t, *J* = 6.0 Hz, 1H), 7.93-7.90 (m, 2H), 7.84-7.75 (m, 3H), 7.58-7.38 (m, 5H), 4.56-4.53 (m, 2H), 2.30-2.25 (m, 2H), 1.06 (t, J = 7.2 Hz, 3H); ^{13}C NMR (100 MHz, DMSO): δ 166.8, 163.1, 153.5, 143.9, 134.7, 131.8, 128.8, 128.1, 127.7, 127.5(d), 42.9, 25.9, 11.1. HRMS-ESI [(m+H$^+$)/z] calculated for $C_{18}H_{19}N_3O_2$: 310.15567; found, 310.15529. (λ_{254}) purity 97.5%, t_R 11.60 mins.

N-(4-(2-propylhydrazine-1-carbonyl)benzyl)benzamide (**2d**). 2 mmol of **2sm** was dissolved in 100 mL ethanol with ultra-sonication aid. To this solution was added 40 mmol of magnesium sulfate and 2 mmol of propanal. From here the reaction proceeded as described in **Series 2 General Procedure** to yield 318 mg (51% yield). ^{1}H NMR (400 MHz, DMSO): δ 9.98 (d, *J* = 6.0 Hz, 1H), 9.11 (t, *J* = 6.0 Hz, 1H), 7.92-7.91 (m, 2H), 7.81-7.79 (m, 2H), 7.56-7.48 (m, 3H), 7.41-7.39 (m, 2H), 5.11-5.07 (m, 1H), 4.53 (d, *J* = 6.0 Hz, 2H), 2.78-2.73 (m, 2H), 1.49-1.44 (m, 2H), 0.92 (t, *J* = 7.6 Hz, 3H); ^{13}C NMR (100 MHz, DMSO): δ 166.7, 165.6, 143.5, 134.7, 132.2, 131.8, 128.8, 127.7, 127.6, 127.4, 53.6, 42.9, 21.3, 12.1. HRMS-ESI [(m+H$^+$)/z] calculated for $C_{18}H_{21}N_3O_2$: 312.17132; found, 312.17127. (λ_{254}) purity >99%, t_R 12.28 mins.

N-(4-(2-pentylhydrazine-1-carbonyl)benzyl)benzamide (**2e**). 2 mmol of **2sm** was dissolved in 100 mL ethanol with ultra-sonication aid. To this solution was added 40 mmol of magnesium sulfate and 2 mmol of pentanal. From here the reaction proceeded as described in **Series 2 General Procedure** to yield 312 mg (46% yield). ^{1}H NMR (400 MHz, DMSO): δ 9.99 (s, 1H), 9.11 (t, *J* = 6.0 Hz, 1H), 7.93-7.91 (m, 2H), 7.81-7.79 (m, 2H), 7.57-7.47 (m, 3H), 7.41-7.39 (m, 2H), 5.07 (s, 1H), 4.53 (d, *J* = 6.0 Hz, 2H), 2.78 (s, 2H), 1.48-1.44 (m, 2H), 1,33-1.29 (m, 4H), 0.88 (t, *J* = 6.8 Hz, 3H); ^{13}C NMR (100 MHz, DMSO): δ 166.8, 165.6, 143.5, 134.7, 132.2, 131.8, 128.8, 127.7, 127.6, 127.5, 51.7, 42.9, 29.4, 27.8, 22.5, 14.4. [(m+H^{+})/z = 340.25]. (λ_{254}) purity >99%, t_R 11.30 mins.

N-(4-(2-(3,3,3-trifluoropropyl)hydrazine-1-carbonyl)benzyl)benzamide (**2f**). 2 mmol of **2sm** was dissolved in 100 mL ethanol with ultra-sonication aid. To this solution was added 40 mmol of magnesium sulfate and 2 mmol of 3,3,3-trifluoropropanal. From here the reaction proceeded as described in **Series 2 General Procedure** to yield 445 mg (61% yield). ^{1}H NMR (400 MHz, DMSO): δ 10.03 (d, *J* = 6.0 Hz, 1H), 9.11 (t, *J* = 6.0 Hz, 1H), 7.92-7.90 (m, 2H), 7.82-7.80 (m, 2H), 7.58-7.48 (m, 3H), 7.42-7.40 (m, 2H), 5.43-5.39 (m, 1H), 4.54 (d, *J* = 6.0 Hz, 2H), 3.05-3.00 (m, 2H), 2.54-2.44 (m, 2H); ^{13}C-HSQC (100MHz, 400 MHz, DMSO) δ 131.8, 128.8, 127.7, 127.6, 127.5, 44.55, 42.8, 32.1. [(m+H^{+})/z = 366.25]. (λ_{254}) purity 97.7%, t_R 10.85 mins.

N-(4-(2-(cyclopropylmethyl)hydrazine-1-carbonyl)benzyl)benzamide (**2g**). 2 mmol of **2sm** was dissolved in 100 mL ethanol with ultra-sonication aid. To this solution was added 40 mmol of magnesium sulfate and 2 mmol of cyclopropanecarbaldehyde. From here the reaction proceeded as described in **Series 2 General Procedure** to yield 415 mg (64% yield). ^{1}H NMR (400 MHz, DMSO): δ 10.06 (s, 1H), 9.13 (s, 1H), 7.93-7.92 (m, 2H), 7.85-7.80 (m, 2H), 7.57-7.47 (m, 3H), 7.41-7.39 (m, 2H), 5.12 (s, 1H), 4.55 (s, 2H), 2.66 (s, 2H), 0.93-0.91 (m, 1H), 0.46-0.44 (m, 2H),

0.16-0.15 (m, 2H); ^{13}C NMR (100 MHz, DMSO): δ 166.8, 165.5, 143.5, 134.7, 132.2, 131.8, 128.8, 127.7, 127.6, 127.5, 56.6, 42.9, 9.95, 3.61. [(m+H$^+$)/z = 324.17]. (λ_{254}) purity 97.4%, t_R 9.27 mins.

N-(4-(2-heptylhydrazine-1-carbonyl)benzyl)benzamide (**2h**). 2 mmol of **2sm** was dissolved in 100 mL ethanol with ultra-sonication aid. To this solution was added 40 mmol of magnesium sulfate and 2 mmol of heptanal. From here the reaction proceeded as described in **Series 2 General Procedure** to yield 345 mg (47% yield). ^{1}H NMR (400 MHz, DMSO): δ 10.00 (s, 1H), 9.12 (t, *J* = 6.0 Hz, 1H), 7.93-7.91 (m, 2H), 7.82-7.80 (m, 2H), 7.57-7.47 (m, 3H), 7.41-7.39 (m, 2H), 5.08-5.05 (m, 1H), 4.54 (d, *J* = 6.0 Hz, 2H), 2.81-2.76 (m, 2H), 1,48-1.44 (m, 2H), 1.34-1.26 (m, 8H), 0.86 (t, *J* = 6.4 Hz, 3H); ^{13}C NMR (100 MHz, DMSO): δ 166.7, 165.6, 143.5, 134.7, 132.2, 131.8, 128.8, 127.7, 127.6, 127.4, 51.7, 42.9, 31.8, 29.1, 28.1, 27.1, 22.6, 14.4. [(m+H$^+$)/z = 368.33]. (λ_{254}) purity >99%, t_R 13.25 mins.

N-(4-(2-octylhydrazine-1-carbonyl)benzyl)benzamide (**2i**). 2 mmol of **2sm** was dissolved in 100 mL ethanol with ultra-sonication aid. To this solution was added 40 mmol of magnesium sulfate and 2 mmol of octanal. From here the reaction proceeded as described in **Series 2 General Procedure** to yield 305 mg (40% yield). ^{1}H NMR (400 MHz, DMSO): δ 10.00 (s, 1H), 9.12 (t, *J* = 6.0 Hz, 1H), 7.93-7.91 (m, 2H), 7.82-7.80 (m, 2H), 7.55-7.46 (m, 3H), 7.41-7.39 (m, 2H), 5.07-5.06 (m, 1H), 4.54 (d, *J* = 5.6 Hz, 2H), 2.80-2.76 (m, 2H), 1.47-1.42 (m, 2H), 1.34-1.25 (m, 10H), 0.86 (t, *J* = 6.4 Hz, 3H); ^{13}C NMR (100 MHz, DMSO): δ 166.7, 165.6, 143.5, 134.7, 132.2, 131.8, 128.8, 127.7, 127.6, 127.4, 51.7, 42.9, 31.7, 29.4, 29.2, 28.1, 27.2, 22.6, 14.4. [(m+H$^+$)/z = 382.33]. (λ_{254}) purity 95.8%, t_R 13.97 mins.

N-(4-(2-hexylhydrazine-1-carbonyl)benzyl)benzamide (**2j**). 2 mmol of **2sm** was dissolved in 100 mL ethanol with ultra-sonication aid. To this solution was added 40 mmol of magnesium sulfate and 2 mmol of hexanal. From here the reaction proceeded as described in **Series 2 General Procedure** to yield 367 mg (52% yield). ^{1}H NMR (400 MHz, DMSO): δ 9.99 (s, 1H), 9.12 (t, *J* = 6.0 Hz, 1H), 7.93-7.91 (m, 2H), 7.81-7.79 (m, 2H), 7.58-7.47 (m, 3H), 7.41-7.39 (m, 2H), 5.08-5.05 (m, 1H), 4.54 (d, *J* = 6.0 Hz, 2H), 2.81-2.76 (m, 2H), 1.49-1.42 (m, 2H), 1.37-1.26 (m, 6H), 0.87 (t, *J* = 6.4 Hz, 3H); ^{13}C NMR (100 MHz, DMSO): δ 166.7, 165.6, 143.5, 134.7, 132.2, 131.8, 128.8, 127.7, 127.6, 127.4, 51.7, 42.9, 31.7, 28.1, 26.8, 22.6, 14.4. [(m+H^{+})/z = 354.33]. (λ_{254}) purity 98.8%, t_R 12.45 mins.

N-(4-(2-decylhydrazine-1-carbonyl)benzyl)benzamide (**2k**). 2 mmol of **2sm** was dissolved in 100 mL ethanol with ultra-sonication aid. To this solution was added 40 mmol of magnesium sulfate and 2 mmol of decanal. From here the reaction proceeded as described in **Series 2 General Procedure** to yield 295 mg (36% yield). ^{1}H NMR (400 MHz, DMSO): δ 9.99 (s, 1H), 9.12 (t, *J* = 6.0 Hz, 1H), 7.93-7.91 (m, 2H), 7.81-7.79 (m, 2H), 7.57-7.54 (m, 3H), 7.41-7.39 (m, 2H), 5.07-5.05 (m, 1H), 4.54 (d, *J* = 6.0 Hz, 2H), 2.80-2.75 (m, 2H), 1.48-1.42 (m, 2H), 1.33-1.25 (m, 14H), 0.86 (t, *J* = 6.8 Hz, 3H); ^{13}C NMR (100 MHz, DMSO): δ 166.7, 165.6, 143.5, 134.7, 132.2, 131.8, 128.8, 127.7, 127.5, 127.4, 51.7, 42.9, 31.8, 29.5(d), 29.2, 28.1, 27.2, 22.6, 14.4. [(m+H^{+})/z = 410.33]. (λ_{254}) purity 98.2%, t_R 15.01 mins.

N-(4-(2-ethylhydrazine-1-carbonyl)benzyl)benzamide (**2l**). 2 mmol of **2sm** was dissolved in 100 mL ethanol with ultra-sonication aid. To this solution was added 40 mmol of magnesium sulfate and 2 mmol of acetaldehyde. From here the reaction proceeded as described in **Series 2 General Procedure** to yield 404 mg (68% yield). ^{1}H NMR (400 MHz, DMSO): δ 10.00 (s, 1H), 9.13-9.11 (m, 1H), 7.93-7.90 (m, 2H), 7.81-7.89 (m, 2H), 7.56-7.47 (m, 3H), 7.42-7.39 (m, 2H), 5.07

(s, 1H), 4.54 (s, 2H), 2.83-2.80 (m, 2H), 1.06-1.02 (m, 3H); ^{13}C NMR (100 MHz, DMSO): δ 166.8, 165.7, 143.5, 134.7, 132.2, 131.8, 128.8, 127.7, 127.6, 127.5, 46.0, 42.9, 13.6. [(m+H$^+$)/z = 298.25]. (λ_{254}) purity 95.6%, t_R 7.71 mins.

N-(4-(2-(cyclobutylmethyl)hydrazine-1-carbonyl)benzyl)benzamide (**2m**). 2 mmol of **2sm** was dissolved in 100 mL ethanol with ultra-sonication aid. To this solution was added 40 mmol of magnesium sulfate and 2 mmol of cyclobutanecarbaldehyde. From here the reaction proceeded as described in **Series 2 General Procedure** to yield 438 mg (65% yield). ^{1}H NMR (400 MHz, DMSO): δ 9.97 (s, 1H), 9.14-9.10 (m, 1H), 7.93-7.91 (m, 2H), 7.80-7.78 (m, 2H), 7.58-7.48 (m, 3H), 7.40-7.38 (m, 2H), 5.06 (s, 1H), 4.53 (d, *J* = 6.0 Hz, 2H), 2.83 (d, *J* = 7.2 Hz, 2H), 2.49-2.43 (m, 1H), 2.05-2.03 (m, 2H), 1.89-1.78 (m, 2H), 1.74-1.65 (m, 2H); ^{13}C NMR (100 MHz, DMSO): δ 166.7, 165.6, 143.5, 134.7, 132.2, 131.8, 128.8, 127.7, 127.5, 127.4, 57.5, 42.9, 34.2, 26.5, 18.8. [(m+H$^+$)/z = 338.17]. (λ_{254}) purity 96.7%, t_R 10.55 mins.

Synthesis of N-(4-(hydrazide)benzyl)cinnamamide Derivatives (3a-3e).

Intermediate formation. Transcinnamic acid (40 mmol) was dissolved in 500 mL of methylene chloride. The apparatus was purged with argon and bubbled through the solution. To this solution was injected 60 mmol of oxalyl chloride and 10 drops of dimethylformamide. The mixture was stirred at room temperature for 3 hours under constant argon flush. The solution was condensed under vacuum and brought to 0°C. A pre-chilled 1:2 mixture of ethyl acetate and water was slowly added followed by addition of potassium carbonate (80 mmol) and methyl 4-(aminomethyl)benzoate HCl (40 mmol). The reaction was brought to room temperature slowly and allowed to stir for 2 additional hours. The water and organic phases were separated, and the water phase washed twice with ethyl acetate. The organic phases were combined and dried under vacuum. A white solid was obtained and used in the next step without further purification.

The product was resuspended in a 2:2:1 solution of methanol, tetrahydrofuran, and water at 0°C. To this solution was cautiously added 48 lithium hydroxide (48 mmol). The solution was allowed to warm to room temperature and stir overnight. Volatiles were removed under vacuum and the residue was acidified with 1 M HCl before extraction with ethyl acetate; volatiles were once again removed under vacuum and lyophilized. The resulting white crystalline powder was used in the next step without further purification. The 4-(cinnamamidomethyl)benzoic acid generated in the above steps was suspended in 400 mL of dimethylformamide, to which was added Hydroxybenzotriazole (80 mmol) and N-N'-Dicyclochexylcarbodiimide (80 mmol). This solution was stirred for 6 hours at RT before addition of hydrazine water salt (48 mmol) at 0°C in one portion. The mixture was allowed to warm to room temperature and stir overnight before being extracted with 1200 mL of water. The water phase was extracted with ethyl acetate twice, and the organic layers were combined and condensed under vacuum. The product (**3sm**) was purified via flash chromatography to yield the corresponding hydrazide that will be used as a starting material for all further reactions for this family (**3a-3e**).

N-(4-(2-ethylhydrazine-1-carbonyl)benzyl)cinnamide (**3a**). 2 mmol of **3sm** was dissolved in 100 mL ethanol with ultra-sonication aid. To this solution was added 40 mmol of magnesium sulfate and 2 mmol of ethanal. From here the reaction proceeded as described in **Series 2 General Procedure** to yield 454 mg (70% yield). ^{1}H NMR (400 MHz, DMSO): δ 10.0 (s, 1H), 8.70 (t, *J* = 5.9 Hz, 1H), 7.80 (d, *J* = 8.2 Hz, 2H), 7.58 (d, *J* = 6.8 Hz, 2H), 7.49 (d, *J* = 15.8 Hz, 1H), 7.43-7.36 (m, 5H), 6.72 (d, *J* = 15.8 Hz, 1H), 5.06 (s, 1H), 4.46 (d, *J* = 6.0 Hz, 2H), 2.85-2.79 (m, 2H), 2.51 (t, *J* = 1.7 Hz, 2H), 1.04 (t, *J* = 7.2 Hz, 3H); ^{13}C NMR (100MHz, DMSO): δ 165.6, 165.5, 143.2, 139.6, 135.3, 132.3, 130.0, 129.4, 128.0, 127.6, 122.4, 46.0, 42.5, 13.6. [$(m+H^{+})/z$ = 324.25]. (λ_{254}) purity 97.5%, t_R 10.38 mins.

N-(4-(2-propylhydrazine-1-carbonyl)benzyl)cinnamamide (**3b**). 2 mmol of **3sm** was dissolved in 100 mL ethanol with ultra-sonication aid. To this solution was added 40 mmol of magnesium sulfate and 2 mmol of propanal. From here the reaction proceeded as described in **Series 2 General Procedure** to yield 546 mg (81% yield). ^{1}H NMR (400 MHz, DMSO): δ 10.00 (s, 1H), 8.70 (t, *J* = 6.0 Hz, 1H), 7.82-7.80 (m, 2H), 7.60-7.58 (m, 2H), 7.50 (d, *J* = 16 Hz, 1H), 7.45-7.37 (m, 5H), 6.72 (d, *J* = 15.6, 1H), 5.11-5.08 (m, 1H), 4.47 (d, *J* = 5.6 Hz, 2H), 2.78-2.74 (m, 2H), 1.51-1.45 (m, 2H), 0.92 (t, *J* = 7.2 Hz, 3H); ^{13}C NMR (100 MHz, DMSO): δ 165.6, 165.5, 143.2, 139.6, 135.3, 132.3, 130.0, 129.4, 128.0, 127.6 (d), 122.4, 53.6, 42.5, 21.3, 12.1. HRMS-ESI [(m+H$^+$)/z] calculated for $C_{20}H_{23}N_3O_2$: 338.18697; found, 338.18726. (λ_{254}) purity 98.4%, t_R 12.42 mins.

N-(4-(2-butylhydrazine-1-carbonyl)benzyl)cinnamide (**3c**). 2 mmol of **3sm** was dissolved in 100 mL ethanol with ultra-sonication aid. To this solution was added 40 mmol of magnesium sulfate and 2 mmol of butanal. From here the reaction proceeded as described in **Series 2 General Procedure** to yield 576 mg (82% yield). ^{1}H NMR (400 MHz, DMSO): δ 10.0 (s, 1H), 8.7 (t, *J* = 6.0 Hz, 1H), 7.8 (d, *J* = 8.3 Hz, 2H), 7.58 (d, *J* = 6.8 Hz, 2H), 7.49 (d, *J* = 15.8 Hz, 1H), 7.43-7.36 (m, 5H), 6.71 (d, *J* = 15.8 Hz, 1H), 5.06 (s, 1H), 4.45 (d, *J* = 6.0 Hz, 2H), 2.80-2.76 (m, 2H), 2.51 (t, *J* = 1.8 Hz, 2H), 1.48-1.41 (m, 2H), 1.40-1.30 (m, 2H), 0.89 (t, *J* = 7.2 Hz, 3H); ^{13}C NMR (100MHz, DMSO): δ 165.5, 165.5, 143.2, 139.6, 135.3, 132.3, 130.0, 129.4, 128.0, 127.6, 122.4, 51.4, 42.5, 30.3, 20.3, 14.4. [(m+H$^+$)/z = 352.25]. (λ_{254}) purity 98.9%, t_R 12.67 mins.

N-(4-(2-pentylhydrazine-1-carbonyl)benzyl)cinnamide (**3d**). 2 mmol of 3sm was dissolved in 100 mL ethanol with ultra-sonication aid. To this solution was added 40 mmol of magnesium sulfate and 2 mmol of pentanal. From here the reaction proceeded as described in **Series 2 General Procedure** to yield 584 mg (80% yield). ^{1}H NMR (400 MHz, DMSO): δ 10.0 (s, 1H),

8.7 (t, *J* = 6.0 Hz, 1H), 7.8 (d, *J* = 8.3 Hz, 2H), 7.58 (d, *J* = 6.8 Hz, 2H), 7.49 (d, *J* = 15.8 Hz, 1H), 7.45-7.35 (m, 5H), 6.71 (d, *J* = 15.8 Hz, 1H), 5.06 (s, 1H), 4.45 (d, *J* = 6.0 Hz, 2H), 2.80-2.75 (m, 2H), 2.51 (t, *J* = 1.8 Hz, 2H), 1.47-1.44 (m, 2H), 1.33-1.29 (m, 4H), 0.88 (t, *J* = 7.2 Hz, 3H); ^{13}C NMR (100MHz, DMSO): δ 165.5, 165.5, 143.2, 139.6, 135.3, 132.3, 130.0, 129.4, 128.0, 127.6, 122.4, 51.7, 42.5, 29.3, 27.8, 22.5, 14.4. [(m+H$^+$)/z = 366.25]. (λ_{254}) purity 97.5%, t_R 13.34 mins.

N-(4-(2-hexylhydrazine-1-carbonyl)benzyl)cinnamamide (**3e**). 2 mmol of **3sm** was dissolved in 100 mL ethanol with ultra-sonication aid. To this solution was added 40 mmol of magnesium sulfate and 2 mmol of hexanal. From here the reaction proceeded as described in **Series 2 General Procedure** to yield 616 mg (81% yield). ^{1}H NMR (400 MHz, DMSO): δ 10.00 (s, 1H), 8.71 (t, J = 6.0 Hz, 1H), 7.82-7.82 (m, 2H), 7.60-7.58 (m, 2H), 7.55 (d, *J* = 16 Hz, 1H), 7.45-7.36 (m, 5H), 6.73 (d, *J* = 15.6 Hz, 1H), 5.07 (s, 1H), 4.47 (d, *J* = 6.0 Hz, 2H), 2.81-2.76 (m, 2H), 1.49-1.41 (m, 2H), 1.37-1.27 (m, 6H), 0.86 (t, *J* = 6.8 Hz, 3H); ^{13}C NMR (100 MHz, DMSO): δ 165.6, 165.5, 143.2, 139.6, 135.3, 132.3, 130.0, 129.4, 128.0, 127.6 (d), 122.4, 51.7, 42.5, 31.7, 28.1, 26.8, 22.6, 14.4. [(m+H$^+$)/z = 380.33]. (λ_{254}) purity 95.5%, t_R 13.62 mins.

Biological Assay Methods

All assays were performed with <0.1% (v/v) DMSO.

HEK293 Lysate Inhibition Assays. HEK293 cells were purchased from ATCC and cultured in Dulbecco's modified eagle's medium with glutamax and 10% (v/v) FBS. Cells were plated in 75cm^2 flasks and incubated at 37°C and 5% CO_2 until ~80% confluent. Cells were harvested, washed, and pelleted, lysed before protein concentration was determined using a Tecan M200 spectrophotometer in a BCA assay, and finally stored at -80°C. Upon need, lysate was thawed

and diluted to 1 mg/mL of protein concentration with HDAC Buffer. HDAC buffer was comprised of 50 mM Tris HCl with 137 mM NaCl, 2.7 mM, and 1 mM $MgCl_2$. The solution was buffered to a pH of 8 and 1 mg/mL BSA was added. 10 µL of this diluted lysate solution was added in 96-well format black U-bottom plates. Serially diluted inhibitor solution was added and a 2 hour pre incubation occurred at 37°C. 50 µM (final) of Acetylated Lysine-Aminomethyl coumarin-BOC in HDAC buffer solution was added and a second 2 hour incubation occurred at 37°C. 5 mg/mL trypsin, 1 µM trichostatin A solution in HDAC buffer was added to quench the reaction. Fluorescence was read at 360 (ex.)/460 (em.) using a Tecan M200 Pro. Data were normalized to control wells containing no inhibitor. IC_{50} values were determined using GraphPad Prism's "log(inhibitor) vs. normalized response – Variable slope" function.

Recombinant HDAC Inhibition Assays. Recombinant HDACs 1, 2, and 3 (BPS Biosciences) were diluted to a concentration of 1 nM in HDAC buffer. 10 uL of this solution was added in 96-well format to black U-bottom plates. 10 uL of serially diluted inhibitor was added and a 2 hour pre incubation occurred at room temperature. 50 µM (final) of Acetylated Lysine-Aminomethyl coumarin-BOC in HDAC buffer solution was added and a second 2 hour incubation occurred at room temperature. 5 mg/mL trypsin, 1 µM trichostatin A solution in HDAC buffer was added to quench the reaction. Fluorescence was read at 360 (ex.)/460 (em.) using a Tecan M200 Pro. Data were normalized to control wells containing no inhibitor. IC_{50} values were determined using GraphPad Prism's built in "log(inhibitor) vs. normalized response – Variable slope" function. K_i values were calculated using the Cheng-Prusoff equation, $K_i = IC_{50}/(1+([Substrate]/K_m))$.

ESI-LCMS Glucuronidation Assays. Mixed gender pooled Human Liver Microsomes (HLMs) were purchased from Xenotech, Lot#H0160. A buffer solution containing 100 mM Tris HCl

buffered to a pH of 7.5 at 37°C was used to dilute HLMs to a concentration of 250 µg/mL. To this solution was added 1 µg/mL (final) of alamethicin and 5 mM $MgCl_2$ (final). This solution was rocked gently at 4°C for 15 minutes to allow pore formation. 180 µL of this solution was added to 10 µL of 5 mM inhibitor + 10 µL of 50 mM UDPGA in H_2O or just 10 µL H_2O. This solution was gently rocked at 37°C for 12 hours before being quenched with a 47:50:3 (v/v/v) solution of water, acetonitrile and formic acid. After a 15 minute centrifugation at 15000g in 37°C conditions, 20 µL of supernatant was directly injected into Thermo LTQ Fleet LCMS.

ESI-LCMS Protocol. An Accucore RP-MS HPLC Column, 2.6 µm particle size, 30x4.6 mm was used throughout these assays. Water and methanol with 0.1% (v/v) formic acid were used as mobile phase. A gradient of 10% methanol 90% water was run isocratically for 2 minutes at 500 µL/min. The gradient then increased to 100% methanol over 15 minutes before returning to 10% methanol 90% water over the next three minutes. Capillary temperature was 350°C, with a spray voltage of 5 kV.

ESI-LCToF HRMS Protocol. A Kinetex C18 column, 5 µm particle size, 25x4.5 mm was used. Water and acetonitrile with 0.1% (v/v) formic acid were used as mobile phase. A gradient of 10% acetonitrile 90% water was run isocratically for 2 minutes at 500 µL/min. The gradient increased to 90% acetonitrile over 15 minutes before returning to 10% acetonitrile 90% water over the next three minutes. Capillary temperature was 245°C, with a spray voltage of 4.5 kV.

Recombinant HDACs 1 and 3 V_{max} Studies. Recombinant human HDACs 1 and 3 were diluted to a concentration of 0.25 nM (final) using HDAC buffer. 100 µL of enzyme solution was added in 96-well format to black U-bottom plates. 100 µL of inhibitor at various concentrations, diluted in HDAC buffer, was added. A 2 hour room temperature pre-incubation

occurred before addition of 20 μL serially diluted Acetylated Lysine-Aminomethyl coumarin-BOC substrate in HDAC buffer. An additional 2 hour room temperature incubation occurred before addition of 20 μL of 5 mg/mL trypsin, 1 μM trichostatin A solution in HDAC buffer to quench the reaction. Fluorescence was read at 360 nm (ex.)/460 nm (em.) using a Tecan M200 Pro. V_{max} and K_m values were determined using GraphPad Prism's Michaelis-Menten function. Corresponding Lineweaver-burke double reciprocal plots were derived from these values and plotted accordingly.

Molecular Docking against HDAC3. Modeling and simulations were performed using MOE 2014.09 (Chemical Computing Group, Inc) using structural pdb: 4A69, HDAC3 bound to human NCOR2 corepressor. Before analysis, proteins were protonated at pH 7.4 and structures energy minimized with heavy atoms constrained using the Amber12:ETH forcefield. Initial surface probe simulations focused on using **3b** as a probe for potential interaction sites, docking to the heterodimers using the entire surface as a target. The surface probe simulations left the protein dimer rigid and flexed the ligand. Initial placement calculated 200 poses using triangle matching with London dG scoring; the top 100 poses were then refined using forcefield and Affinity dG scoring. The consensus docking site was determined using Protein Ligand Interaction Fingerprint (PLIF) analysis. The HDAC3 bound to corepressor structure described above was used to estimate the propensity for ligand binding (PLB) for the entire surface. Settings for MOE SiteFinder were: Probe Radius1: 1.5, probe radius 2: 1.8, isolated donor/acceptor: 3, connection distance: 2.5, minimum site size: 3, radius: 3. The consensus site between the surface probe and PLB analysis was used to create docking dummies for site focused docking simulations with an additional 4.5 angstrom radii. The focused dock used induced fit for the protein, allowing protein and ligand flexing. Initial placement calculated 200 poses using triangle matching with

London dG scoring, the top 100 poses were then refined using forcefield and Affinity dG scoring.

MV4-11 EC_{50} Analysis. MV4-11 cells were purchased from ATCC. The cells were grown according to ATCC protocol in Iscove's Modified Deulbecco's Medium with 10% Fetal Bovine Serum. Cells were grown in 37°C environments with 5% CO_2. Cells were plated at 20k cells/well in 96-well clear U-bottom plates and pre-incubated for 24 hours. Addition of serially diluted inhibitor (in medium) was performed followed by 48 hours of additional incubation. Addition of CellTiter-Blue occurred to a final concentration of 0.125 mg/mL. The mixture was allowed to incubate until sufficient color changed occurred. Cell viability was measured as a function of resorfuin intensity using a Tecan M200 Pro spectrophotometer, 560 nm (ex.)/590 nm (em.). Data were normalized to control wells and background was removed. EC_{50} values were determined using GraphPad Prism's "log(inhibitor) vs. normalized response – Variable slope" function.

Western Blot Analysis of MV4-11 Cells. MV4-11 cells were cultured as described above. Cells were plated at 500k cells/mL x 3 mL in clear, flat bottom 6 well plates. Cells were pre-incubated for 24 hours before addition of inhibitor at various concentrations. The cells were allowed to incubate for 24 additional hours before being harvested, pelleted, and stored at -80°C. Cell pellets were lysed with RIPA buffer. RIPA buffer is comprised of 50 mM Tris Base, 150 mM NaCl, 5 mM EDTA, 0.1% (v/v) SDS, 0.5% (v/v) Sodium Deoxycholate, and 1% (v/v) Triton-x-100. After lysing, the suspension is ultra-sonicated and centrifuged at 15000 RPM for 15 minute at 4°C. 80 µL of supernatant was mixed with 40 µL of 15:85 (v/v) β-mercaptoethanol:LDS solution. The mixture was heated at 90°C for 15 minutes and stored for loading at -20°C. Prior to loading, the solution was flash thawed at 90°C. Lysates were run on

Invitrogen NuPAGE 4-12% Bis-Tris 15 well gels at 170V for approximately 60 minutes in MES buffer. Gels were transferred to methylcellulose and ran at 30V for 180 minutes. Primary antibodies, all purchased from Santa Cruz Biotechnology, except actin, purchased from Sigma, were added in 5% (w/v) milk or 5% (w/v) Bovine Serum Albumin fraction V. The respective antibody was incubated with the cellulose overnight at 4°C before addition of secondary antibody in 5% (w/v) milk or 5% (w/v) Bovine Serum Albumin. Images were acquired using a GE ImageQuant LAS 4000. Global lighting adjustments of resulting images were made using Adobe Photoshop CC. Quantification was performed using Image Studio Lite 4.0.

HEK293 and HeLa EC_{50} Analysis. HEK293 and HeLa cells were purchased from ATCC. Cells were grown as described above. Cells were plated at 20k cells/well in 96-well clear U-bottom plates and pre-incubated for 24 hours. Addition of serially diluted inhibitor (in medium) was performed followed by 48 hours of additional incubation. Addition of CellTiter-Blue occurred to a final concentration of 0.125 mg/mL. The mixture was allowed to incubate until sufficient color changed occurred. Cell viability was measured as a function of resorufin intensity using a Tecan M200 Pro spectrophotometer, 560 nm (ex.)/590 nm (em.).

Human Peripheral Blood Mononuclear Cell Analysis. Human PBMCs were graciously donated from Dr. Nathan Dolloff's laboratory. Cells were flash thawed from liquid nitrogen using RPMI-1640 media + Glutamax and 15% Fetal Bovine Serum and allowed to incubate overnight at 37°C, 5% CO_2. Cells were centrifuged at 1000 RPM for 5 minutes. Pelleted, healthy cells were reseeded at 50k cells/well and treated immediately with serially diluted inhibitors (diluted in medium). Cells were allowed to incubate with inhibitor or vehicle for 24 hours before addition of 0.125 mg/mL (final) CellTiter-Blue. The mixture was allowed to incubate until sufficient color changed occurred. Cell viability was measured as a function of

resorufin intensity using a Tecan M200 Pro spectrophotometer, 560 nm (ex.)/590 nm (em.). Data were normalized to control wells and background was subtracted.

ASSOCIATED CONTENT

Supporting Information. The following are made available free of charge via the internet at http://pubs.acs.org

Supporting Tables S1-2

Supporting Figures S1-4

Corresponding Author Information

*C. James Chou: Phone (843) 792-1289. Email: chouc@musc.edu

Author Contributions

ǂAuthors contributed equally and should be both considered first authors. The manuscript was written by JJM. Synthesis of substrates was performed by CZ and JJM. Assays and biological data collection were performed by JJM, ESI, and JL. YKP and JJM performed the molecular modeling. All authors have given approval to the final version of the manuscript.

Acknowledgements

The authors would like to acknowledge C.C. Beeson and R.G. Schnellmann for their continued support throughout the authoring and experimental progress of this manuscript. The authors would also like to acknowledge A. Nagel for her support with HRMS.

Funding Sources

This work was supported by the National Institute of Health/National Cancer Institute (CA163452 to C.J.C.), the National Institute of General Medical Sciences (8P20GM103542-02) from the National Institutes of Health, South Carolina Clinical and Translational Research Institute UL1RR029882, and in part by pilot research funding from an American Cancer Society Institutional Research Grant awarded to the Hollings Cancer Center, Medical University of South Carolina.

The authors declare no competing financial interest.

ABBREVIATIONS

AcOEt, Ethyl Acetate; DCC, *N-N'*-Dicyclochexylcarbodiimide; DMF, dimethylformamide; EtOH, Ethanol; HDAC, Histone Deacetylase; HH3, Histone H3; HH4, Histone H4; HOBt, Hydroxybenzotriazole; HLM, Human Liver Microsomes, LiOH, Lithium Hydroxide; $MgSO_4$, Magnesium Sulfate; MeOH, Methanol; $NaBH_3CN$, MM, Multiple Myeloma; Sodium Cyanoborohydride; PTM, Post-Translational Modification, rt, Room Temperature

REFERENCES

1. Falkenberg, K. J.; Johnstone, R. W. Histone deacetylases and their inhibitors in cancer, neurological diseases and immune disorders. *Nat. Rev. Drug Discovery.* **2014,** *13*, 673-691.

2. Gregoretti, I. V.; Lee, Y. M.; Goodson, H. V. Molecular evolution of the histone deacetylase family: functional implications of phylogenetic analysis. *J. Mol. Biol.* **2004,** *338*, 17-31.

3. Gallinari, P.; Marco, S. D.; Jones, P.; Pallaoro, M.; Steinkuhler, C. HDACs, histone deacetylation and gene transcription: from molecular biology to cancer therapeutics. *Cell Res.* **2007,** *17*, 195-211.

4. Richon, V. M.; Sandhoff, T. W.; Rifkind, R. A.; Marks, P. A. Histone deacetylase inhibitor selectively induces p21WAF1 expression and gene-associated histone acetylation. *Proc. Natl. Acad. Sci. U.S.A.* **2000,** *97*, 10014-10019.

5. Sambucetti, L. C.; Fischer, D. D.; Zabludoff, S.; Kwon, P. O.; Chamberlin, H.; Trogani, N.; Xu, H.; Cohen, D. Histone deacetylase inhibition selectively alters the activity and expression of cell cycle proteins leading to specific chromatin acetylation and antiproliferative effects. *J. Biol. Chem.* **1999,** *274*, 34940-34947.

6. Zhang, Y.; Li, N.; Caron, C.; Matthias, G.; Hess, D.; Khochbin, S.; Matthias, P. HDAC-6 interacts with and deacetylates tubulin and microtubules in vivo. *EMBO J.* **2003,** *22*, 1168-1179.

7. Fonseca, R. The aging memory: Modulating epigenetic modifications to improve cognitive function. *Neurobiol. Learn. Mem*. [Online early access]. DOI: 10.1016/j.nlm.2016.07.002. Published Online: September 2016.

8. Benito, E.; Urbanke, H.; Ramachandran, B.; Barth, J.; Halder, R.; Awasthi, A.; Jain, G.; Capece, V.; Burkhardt, S.; Navarro-Sala, M.; Nagarajan, S.; Schutz, A. L.; Johnsen, S. A.; Bonn, S.; Luhrmann, R.; Dean, C.; Fischer, A. HDAC inhibitor-dependent transcriptome and memory reinstatement in cognitive decline models. *J. Clin. Invest.* **2015,** *125*, 3572-3584.

9. Rumbaugh, G.; Sillivan, S. E.; Ozkan, E. D.; Rojas, C. S.; Hubbs, C. R.; Aceti, M.; Kilgore, M.; Kudugunti, S.; Puthanveettil, S. V.; Sweatt, J. D.; Rusche, J.; Miller, C. A. Pharmacological selectivity within class I histone deacetylases predicts effects on synaptic function and memory rescue. *Neuropsychopharmacology.* **2015,** *40*, 2307-2316.

10. Sharma, S.; Taliyan, R.; Ramagiri, S. Histone deacetylase inhibitor, Trichostatin A, improves learning and memory in high-fat diet-induced cognitive deficits in mice. *J. Mol. Neurosci.* **2015,** *56*, 1-11.

11. Sharma, S.; Taliyan, R. Synergistic effects of GSK-3beta and HDAC inhibitors in intracerebroventricular streptozotocin-induced cognitive deficits in rats. *Naunyn-Schmiedeberg's Arch. Pharmacol.* **2015,** *388*, 337-349.

12. Wagner, F. F.; Zhang, Y. L.; Fass, D. M.; Joseph, N.; Gale, J. P.; Weiwer, M.; McCarren, P.; Fisher, S. L.; Kaya, T.; Zhao, W. N.; Reis, S. A.; Hennig, K. M.; Thomas, M.; Lemercier, B. C.; Lewis, M. C.; Guan, J. S.; Moyer, M. P.; Scolnick, E.; Haggarty, S. J.; Tsai, L. H.; Holson, E. B. Kinetically selective inhibitors of histone deacetylase 2 (HDAC2) as cognition enhancers. *Chem. Sci.* **2015,** *6*, 804-815.

13. Hsing, C. H.; Hung, S. K.; Chen, Y. C.; Wei, T. S.; Sun, D. P.; Wang, J. J.; Yeh, C. H. Histone deacetylase inhibitor Trichostatin A ameliorated endotoxin-induced neuroinflammation and cognitive dysfunction. *Mediators Inflammation.* **2015,** *2015*, 163140.

14. Penney, J.; Tsai, L. H. Histone deacetylases in memory and cognition. *Sci. Signaling.* **2014,** *7*, re12.

15. Dobreva, Z. G.; Grigorov, B. G.; Stanilova, S. A. Suppression of IL-12p40-related regulatory cytokines by suberoylanilide hydroxamic acid an inhibitor of histone deacetylases. *Immunopharmacol. Immunotoxicol.* **2016,** *38*, 281-285.

16. Leus, N. G.; Zwinderman, M. R.; Dekker, F. J. Histone deacetylase 3 (HDAC 3) as emerging drug target in NF-kappaB-mediated inflammation. *Curr. Opin. Chem. Biol.* **2016,** *33*, 160-168.

17. Pham, T. X.; Park, Y. K.; Lee, J. Y. Anti-inflammatory effects of spirulina platensis Extract via the modulation of histone deacetylases. *Nutrients.* **2016,** *8*.

18. Somanna, N. K.; Valente, A. J.; Krenz, M.; McDonald, K. S.; Higashi, Y.; Noda, M.; Chandrasekar, B. Histone deacetyltransferase inhibitors Trichostatin A and Mocetinostat

differentially regulate MMP9, IL-18 and RECK expression, and attenuate Angiotensin II-induced cardiac fibroblast migration and proliferation. *Hypertens. Res.* **2016**. [Online early access]. DOI: 10.1038/hr.2016.54. Published Online: Jun 9, 2016.

19. Leus, N. G.; van der Wouden, P. E.; van den Bosch, T.; Hooghiemstra, W. T.; Ourailidou, M. E.; Kistemaker, L. E.; Bischoff, R.; Gosens, R.; Haisma, H. J.; Dekker, F. J. HDAC 3-selective inhibitor RGFP966 demonstrates anti-inflammatory properties in RAW 264.7 macrophages and mouse precision-cut lung slices by attenuating NF-kappaB p65 transcriptional activity. *Biochem. Pharmacol.* **2016,** *108*, 58-74.

20. Patnaik, A.; Rowinsky, E. K.; Villalona, M. A.; Hammond, L. A.; Britten, C. D.; Siu, L. L.; Goetz, A.; Felton, S. A.; Burton, S.; Valone, F. H.; Eckhardt, S. G. A phase I study of pivaloyloxymethyl butyrate, a prodrug of the differentiating agent butyric acid, in patients with advanced solid malignancies. *Clin. Cancer Res.* **2002,** *8*, 2142-2148.

21. Gojo, I.; Jiemjit, A.; Trepel, J. B.; Sparreboom, A.; Figg, W. D.; Rollins, S.; Tidwell, M. L.; Greer, J.; Chung, E. J.; Lee, M. J.; Gore, S. D.; Sausville, E. A.; Zwiebel, J.; Karp, J. E. Phase 1 and pharmacologic study of MS-275, a histone deacetylase inhibitor, in adults with refractory and relapsed acute leukemias. *Blood.* **2007,** *109*, 2781-2790.

22. Kummar, S.; Gutierrez, M.; Gardner, E. R.; Donovan, E.; Hwang, K.; Chung, E. J.; Lee, M. J.; Maynard, K.; Kalnitskiy, M.; Chen, A.; Melillo, G.; Ryan, Q. C.; Conley, B.; Figg, W. D.; Trepel, J. B.; Zwiebel, J.; Doroshow, J. H.; Murgo, A. J. Phase I trial of MS-275, a histone deacetylase inhibitor, administered weekly in refractory solid tumors and lymphoid malignancies. *Clin. Cancer. Res.* **2007,** *13*, 5411-5417.

23. Garcia-Manero, G.; Assouline, S.; Cortes, J.; Estrov, Z.; Kantarjian, H.; Yang, H.; Newsome, W. M.; Miller, W. H., Jr.; Rousseau, C.; Kalita, A.; Bonfils, C.; Dubay, M.; Patterson,

T. A.; Li, Z.; Besterman, J. M.; Reid, G.; Laille, E.; Martell, R. E.; Minden, M. Phase 1 study of the oral isotype specific histone deacetylase inhibitor MGCD0103 in leukemia. *Blood.* **2008,** *112*, 981-989.

24. Siu, L. L.; Pili, R.; Duran, I.; Messersmith, W. A.; Chen, E. X.; Sullivan, R.; MacLean, M.; King, S.; Brown, S.; Reid, G. K.; Li, Z.; Kalita, A. M.; Laille, E. J.; Besterman, J. M.; Martell, R. E.; Carducci, M. A. Phase I study of MGCD0103 given as a three-times-per-week oral dose in patients with advanced solid tumors. *J. Clin. Oncol.* **2008,** *26*, 1940-1947.

25. Reid, T.; Valone, F.; Lipera, W.; Irwin, D.; Paroly, W.; Natale, R.; Sreedharan, S.; Keer, H.; Lum, B.; Scappaticci, F.; Bhatnagar, A. Phase II trial of the histone deacetylase inhibitor pivaloyloxymethyl butyrate (Pivanex, AN-9) in advanced non-small cell lung cancer. *Lung Cancer.* **2004,** *45*, 381-386.

26. Ramalingam, S. S.; Belani, C. P.; Ruel, C.; Frankel, P.; Gitlitz, B.; Koczywas, M.; Espinoza-Delgado, I.; Gandara, D. Phase II study of belinostat (PXD101), a histone deacetylase inhibitor, for second line therapy of advanced malignant pleural mesothelioma. *J. Thorac. Oncol.* **2009,** *4*, 97-101.

27. Duvic, M.; Talpur, R.; Ni, X.; Zhang, C.; Hazarika, P.; Kelly, C.; Chiao, J. H.; Reilly, J. F.; Ricker, J. L.; Richon, V. M.; Frankel, S. R. Phase 2 trial of oral vorinostat (suberoylanilide hydroxamic acid, SAHA) for refractory cutaneous T-cell lymphoma (CTCL). *Blood.* **2007,** *109*, 31-39.

28. Olsen, E. A.; Kim, Y. H.; Kuzel, T. M.; Pacheco, T. R.; Foss, F. M.; Parker, S.; Frankel, S. R.; Chen, C.; Ricker, J. L.; Arduino, J. M.; Duvic, M. Phase IIb multicenter trial of vorinostat in patients with persistent, progressive, or treatment refractory cutaneous T-cell lymphoma. *J. Clin. Oncol.* **2007,** *25*, 3109-3115.

29. Crump, M.; Coiffier, B.; Jacobsen, E. D.; Sun, L.; Ricker, J. L.; Xie, H.; Frankel, S. R.; Randolph, S. S.; Cheson, B. D. Phase II trial of oral vorinostat (suberoylanilide hydroxamic acid) in relapsed diffuse large-B-cell lymphoma. *Ann. Oncol.* **2008,** *19*, 964-969.

30. Vansteenkiste, J.; Van Cutsem, E.; Dumez, H.; Chen, C.; Ricker, J. L.; Randolph, S. S.; Schoffski, P. Early phase II trial of oral vorinostat in relapsed or refractory breast, colorectal, or non-small cell lung cancer. *Invest. New Drugs.* **2008,** *26*, 483-488.

31. Woyach, J. A.; Kloos, R. T.; Ringel, M. D.; Arbogast, D.; Collamore, M.; Zwiebel, J. A.; Grever, M.; Villalona-Calero, M.; Shah, M. H. Lack of therapeutic effect of the histone deacetylase inhibitor vorinostat in patients with metastatic radioiodine-refractory thyroid carcinoma. *J. Clin. Endocrinol. Metab.* **2009,** *94*, 164-170.

32. Shah, M. H.; Binkley, P.; Chan, K.; Xiao, J.; Arbogast, D.; Collamore, M.; Farra, Y.; Young, D.; Grever, M. Cardiotoxicity of histone deacetylase inhibitor depsipeptide in patients with metastatic neuroendocrine tumors. *Clin. Cancer Res.* **2006,** *12*, 3997-4003.

33. Stadler, W. M.; Margolin, K.; Ferber, S.; McCulloch, W.; Thompson, J. A. A phase II study of depsipeptide in refractory metastatic renal cell cancer. *Clin. Genitourin. Cancer.* **2006,** *5*, 57-60.

34. Odenike, O. M.; Alkan, S.; Sher, D.; Godwin, J. E.; Huo, D.; Brandt, S. J.; Green, M.; Xie, J.; Zhang, Y.; Vesole, D. H.; Stiff, P.; Wright, J.; Larson, R. A.; Stock, W. Histone deacetylase inhibitor romidepsin has differential activity in core binding factor acute myeloid leukemia. *Clin. Cancer Res.* **2008,** *14*, 7095-7101.

35. Shen, S.; Kozikowski, A. P. Why hydroxamates may not be the best histone deacetylase inhibitors--what some may have forgotten or would rather forget? *ChemMedChem.* **2016,** *11*, 15-21.

36. Kang, S. P.; Ramirez, J.; House, L.; Zhang, W.; Mirkov, S.; Liu, W.; Haverfield, E.; Ratain, M. J. A pharmacogenetic study of vorinostat glucuronidation. *Pharmacogenet. Genomics* **2010,** *20*, 638-641.

37. Wong, N. S.; Seah, E.; Wang, L. Z.; Yeo, W. L.; Yap, H. L.; Chuah, B.; Lim, Y. W.; Ang, P. C.; Tai, B. C.; Lim, R.; Goh, B. C.; Lee, S. C. Impact of UDP-gluconoryltransferase 2B17 genotype on vorinostat metabolism and clinical outcomes in Asian women with breast cancer. *Pharmacogenet. Genomics.* **2011,** *21*, 760-768.

38. Wang, L. Z.; Ramirez, J.; Yeo, W.; Chan, M. Y.; Thuya, W. L.; Lau, J. Y.; Wan, S. C.; Wong, A. L.; Zee, Y. K.; Lim, R.; Lee, S. C.; Ho, P. C.; Lee, H. S.; Chan, A.; Ansher, S.; Ratain, M. J.; Goh, B. C. Glucuronidation by UGT1A1 is the dominant pathway of the metabolic disposition of belinostat in liver cancer patients. *PLoS One.* **2013,** *8*, e54522.

39. Moore, D. Panobinostat (Farydak): A novel option for the treatment of relapsed or relapsed and refractory multiple myeloma. *Pharmacy and Therapeutics.* **2016,** *41*, 296-300.

40. Mulder, G. J.; Meerman, J. H. Sulfation and glucuronidation as competing pathways in the metabolism of hydroxamic acids: the role of N,O-sulfonation in chemical carcinogenesis of aromatic amines. *Environ. Health Perspect.* **1983,** *49*, 27-32.

41. Zhang, Q.; Wu, H.; Wen, C.; Sun, F.; Yang, X.; Hu, L. Metabolic changes in rats after intragastric administration of MGCD0103 (Mocetinostat), a HDAC class I inhibitor. *Int. J. Clin. Exp. Pathol.* **2015,** *8*, 9320-9325.

42. Wang, Y.; Stowe, R. L.; Pinello, C. E.; Tian, G.; Madoux, F.; Li, D.; Zhao, L. Y.; Li, J. L.; Wang, Y.; Wang, Y.; Ma, H.; Hodder, P.; Roush, W. R.; Liao, D. Identification of histone deacetylase inhibitors with benzoylhydrazide scaffold that selectively inhibit class I histone deacetylases. *Chem. Biol.* **2015,** *22*, 273-284.

43. Summers, A. R.; Fischer, M. A.; Stengel, K. R.; Zhao, Y.; Kaiser, J. F.; Wells, C. E.; Hunt, A.; Bhaskara, S.; Luzwick, J. W.; Sampathi, S.; Chen, X.; Thompson, M. A.; Cortez, D.; Hiebert, S. W. HDAC3 is essential for DNA replication in hematopoietic progenitor cells. *J. Clin. Invest. 123*, 3112-3123.

44. Walsky, R. L.; Bauman, J. N.; Bourcier, K.; Giddens, G.; Lapham, K.; Negahban, A.; Ryder, T. F.; Obach, R. S.; Hyland, R.; Goosen, T. C. Optimized assays for human UDP-glucuronosyltransferase (UGT) activities: altered alamethicin concentration and utility to screen for UGT inhibitors. *Drug Metab. Dispos.* **2012,** *40*, 1051-1065.

45. Parise, R. A.; Holleran, J. L.; Beumer, J. H.; Ramalingam, S.; Egorin, M. J. A liquid chromatography–electrospray ionization tandem mass spectrometric assay for quantitation of the histone deacetylase inhibitor, vorinostat (suberoylanilide hydroxamicacid, SAHA), and its metabolites in human serum. *J. Chromatogr. B: Anal. Technol. Biomed. Life Sci.* **2006,** *840*, 108-115.

46. Richon, V. M. Cancer biology: mechanism of antitumour action of vorinostat (suberoylanilide hydroxamic acid), a novel histone deacetylase inhibitor. *Br. J. Cancer.* **2006,** *95*, S2-S6.

47. Matsuo, Y.; MacLeod, R. A.; Uphoff, C. C.; Drexler, H. G.; Nishizaki, C.; Katayama, Y.; Kimura, G.; Fujii, N.; Omoto, E.; Harada, M.; Orita, K. Two acute monocytic leukemia (AML-M5a) cell lines (MOLM-13 and MOLM-14) with interclonal phenotypic heterogeneity showing MLL-AF9 fusion resulting from an occult chromosome insertion, ins(11;9)(q23;p22p23). *Leukemia.* **1997,** *11*, 1469-1477.

48. Birnie, G. D. The HL60 cell line: a model system for studying human myeloid cell differentiation. *Br. J. Cancer, Suppl.* **1988,** *9*, 41-45.

49. Stong, R. C.; Korsmeyer, S. J.; Parkin, J. L.; Arthur, D. C.; Kersey, J. H. Human acute leukemia cell line with the t(4;11) chromosomal rearrangement exhibits B lineage and monocytic characteristics. *Blood.* **1985,** *65*, 21-31.

50. Andersson, L. C.; Nilsson, K.; Gahmberg, C. G. K562--a human erythroleukemic cell line. *Int. J. Cancer.* **1979,** *23*, 143-147.

51. Quentmeier, H.; Reinhardt, J.; Zaborski, M.; Drexler, H. G. FLT3 mutations in acute myeloid leukemia cell lines. *Leukemia.* **2003,** *17*, 120-124.

52. Grofova, M.; Popovic, M.; Ogura, H.; Matoska, J.; Lizonova, A.; Nilsson, K.; Kuzela, S. The retrovirus particles in human myeloma cells RPMI8226: morphological, biochemical, immunological and infective transmission studies. *Neoplasma.* **1978,** *25*, 423-437.

53. Vickers, C. J.; Olsen, C. A.; Leman, L. J.; Ghadiri, M. R. Discovery of HDAC inhibitors that lack an active site Zn(2+)-binding functional group. *ACS Med. Chem. Lett.* **2012,** *3*, 505-508.

Chart 1. FDA Approved HDAC Inhibitors

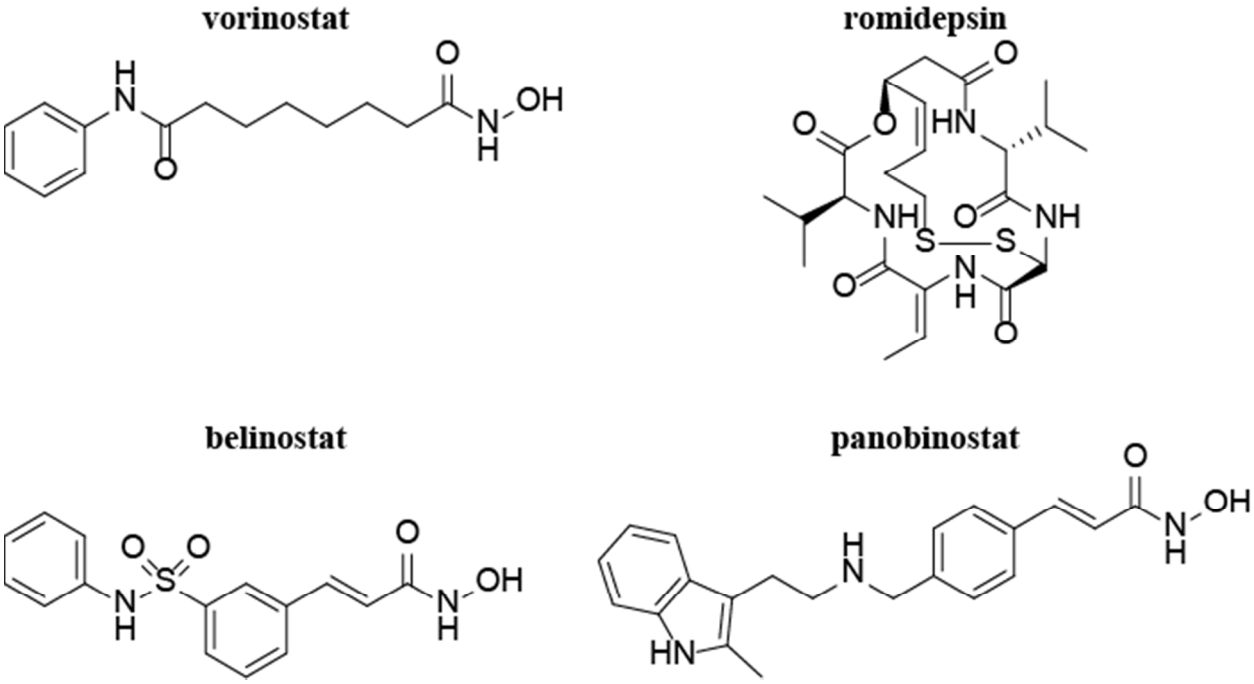

Scheme 1. Butylhydrazide Derivatives Synthesis[a]

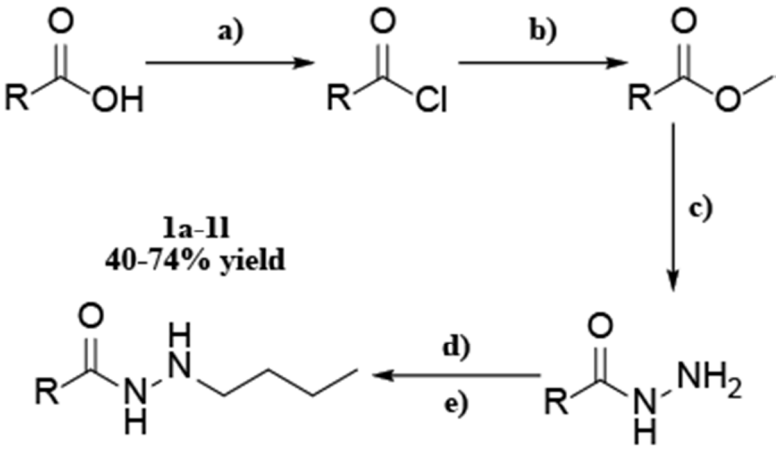

[a]Reagents and conditions: (a) methylene chloride, rt, oxalyl chloride, cat. DMF; (b) MeOH, rt; (c) MeOH, reflux, $NH_2NH_2 \cdot H_2O$; (d) EtOH, reflux, butaldehyde, $MgSO_4$; (e) MeOH, rt, $NaBH_3CN$, conc. HCl

Table 1. In vitro inhibition of recombinant HEK293 lysates and recombinant HDAC3 for series 1 inhibitors[a]

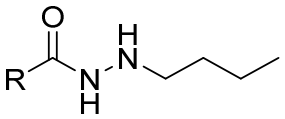

Name	R Group	IC_{50}[a] (nM)		Name	R Group	IC_{50}[a] (nM)	
		HDAC3	HEK293			HDAC3	HEK293
1a	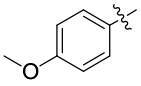	**156.7** ± 28.55	**727.3** ± 10.75	**1g**		**5001** ± 372.5	**>10,000**
1b	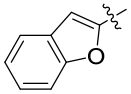	**1362** ± 197.3	**1688** ± 38.05	**1h**	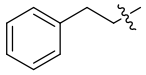	**1892** ± 227.3	**>10,000**
1c	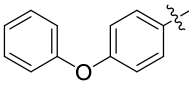	**311.7** ± 42.82	**1691** ± 298.3	**1i**	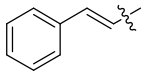	**294.5** ± 32.64	**1440** ± 86.09
1d		**1547** ± 429.8	**4676** ± 909.0	**1j**	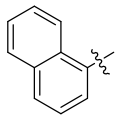	**>10,000**	**>10,000**
1e	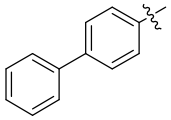	**68.85** ± 9.39	**1307** ± 210.0	**1k**	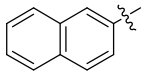	**892.0** ± 72.47	**2844** ± 948.0
1f		**903.9** ± 154.3	**3461** ± 669.0	**1l**	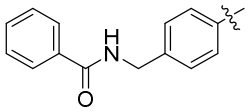	**8.56** ± 2.06	**260.6** ± 8.68

[a]IC_{50} values (bold) are the mean of at least three experiments ± the Standard Error of the Mean.

Scheme 2. N-(4-(hydrazide)benzyl)benzamide Derivatives Synthesis[a]

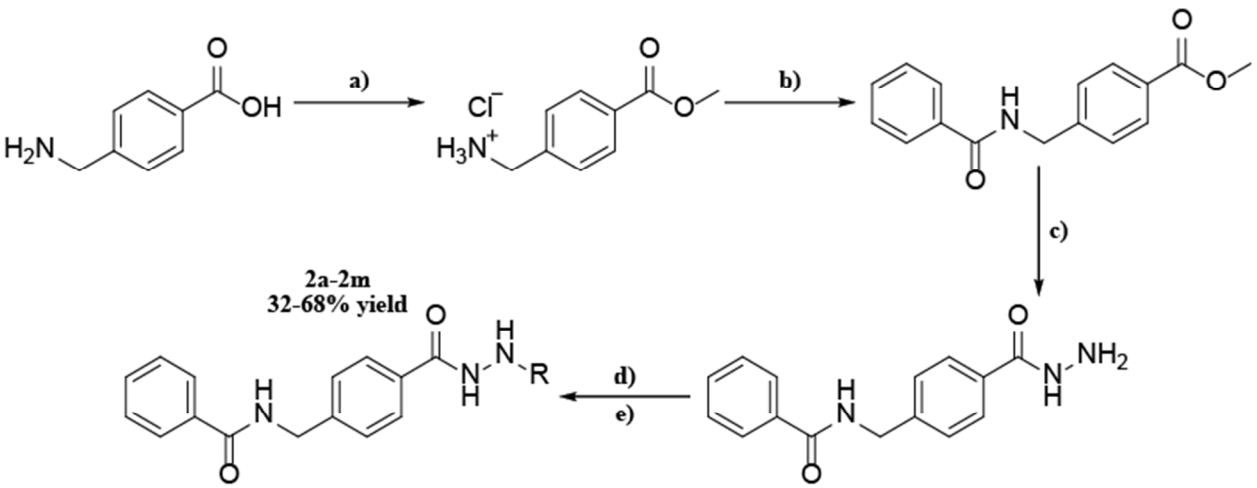

[a]Reagents and conditions: (a) MeOH, reflux, conc. HCl; (b) AcOEt:H_2O (1:1), rt, K_2CO_3; (c) MeOH, reflux, $NH_2NH_2 \cdot H_2O$; (d) EtOH, rt, aldehyde of interest, $MgSO_4$; (e) MeOH, $NaBH_3CN$, conc. HCl

Table 2. In vitro inhibition of recombinant HEK293 lysates and recombinant HDAC3 for series 2 inhibitors[a]

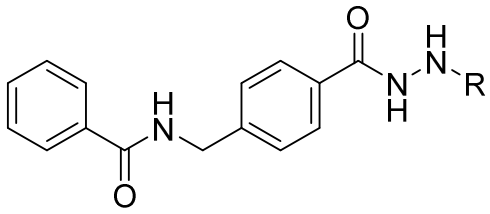

Name	R Group	IC_{50}[a] (nM)		Name	R Group	IC_{50}[a] (nM)	
		HDAC3	HEK293			HDAC3	HEK293
2a	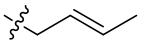	**1533** ± 227.5	**>10,000**	**2h**	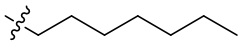	**568.7** ± 84.9	**2161** ± 895.5
2b		**>10,000**	**>10,000**	**2i**	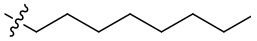	**1093** ± 334.4	**>10,000**
2c	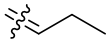	**>10,000**	**>10,000**	**2j**	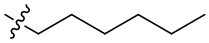	**184.1** ± 74.54	**550.2** ± 133.9
2d	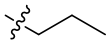	**3.47** ± 0.48	**155.3** ± 27.64	**2k**	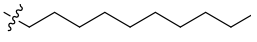	**>10,000**	**>10,000**
2e	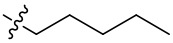	**18.74** ± 4.3	**263.6** ± 28.52	**2l**		**187.3** ± 0.6	**427.1** ± 110.5
2f	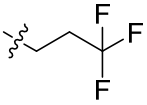	**69.10** ± 0.52	**1229** ± 136.5	**2m**	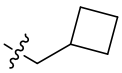	**84.44** ± 7.22	**1883** ± 212.4
2g	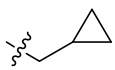	**39.93** ± 0.25	**1621** ± 196				

[a]IC50 values (bold) are the mean of at least three experiments ± the Standard Error of the Mean.

Scheme 3. N-(4-(hydrazide)benzyl)cinnamamide Derivatives Synthesis[a]

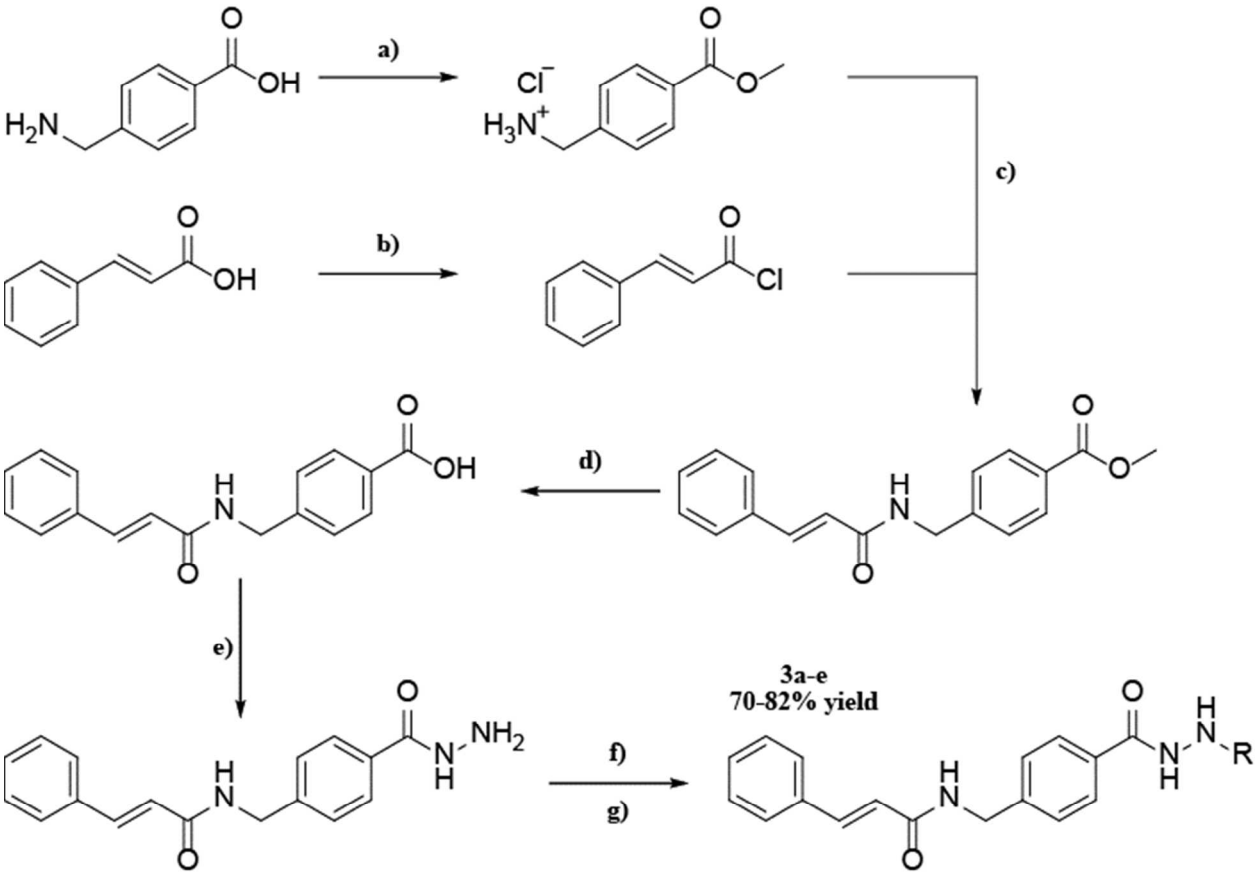

[a]Reagents and conditions: (a) MeOH, reflux, conc. HCl; (b) DCM, rt, Oxalyl Chloride, cat. DMF; (c) EtOAc:H_2O (1:1), rt, K_2CO_3; (d) MeOH:H_2O:THF (2:1:2), rt, LiOH; (e) DMF, rt, HOBt, DCC; (f) DMF, 0°C, $NH_2NH_2 \cdot H_2O$; (g) EtOH, rt, aldehyde of interest, $MgSO_4$; (h) MeOH, rt, $NaBH_3CN$, conc. HCl

Table 3. In vitro inhibition of recombinant HDACs 1, 2, and 3 and HEK293 Lysate for series 3 inhibitors[a]

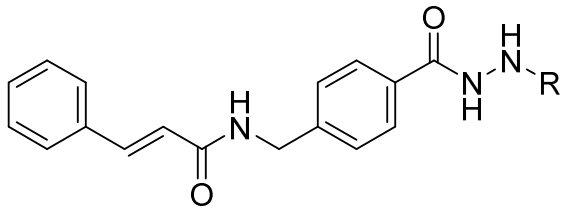

Name	R Group	IC_{50}[a] (nM)			
		HDAC1	**HDAC2**	**HDAC3**	**HEK293**
3a		**29.49** ± 10.71	**76.57** ± 9.74	**19.71** ± 1.41	**171.1** ± 34.23
3b	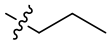	**11.81** ± 4.16	**95.45** ± 34.15	**0.95** ± 0.19	**124.4** ± 14.02
3c	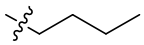	**60.17** ± 20.97	**70.03** ± 26.38	**3.67** ± 2.86	**494.3** ± 209.6
3d	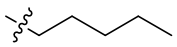	**47.36** ± 16.79	**99.56** ± 17.44	**32.55** ± 1.15	**690.7** ± 54.67
3e	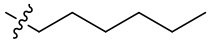	**81.36** ± 11.96	**139.2** ± 29.9	**149.8** ± 81.63	**1718** ± 139.1

[a]IC_{50} values (bold) are the mean of at least three experiments ± the Standard Error of the Mean.

Table 4. Leukemia and myeloma cell line data for **3b**

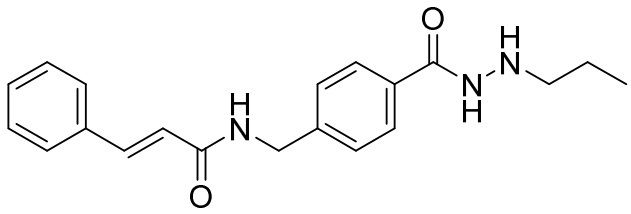

EC_{50}[a] (nM)					
MV4-11	**Molm14**	**RS4-11**	**K562**	**HL-60**	**RPMI-8226**
36.37 ± 8.83	**76.64** ± 18.37	**151.7** ± 44.29	**2160** ± 128.3	**>10,000**	**>10,000**

[a]EC_{50} values (bold) are the mean of at least two experiments ± the Standard Error of the Mean.

Figure 1. ESI-LCMS glucuronidation assay[a]

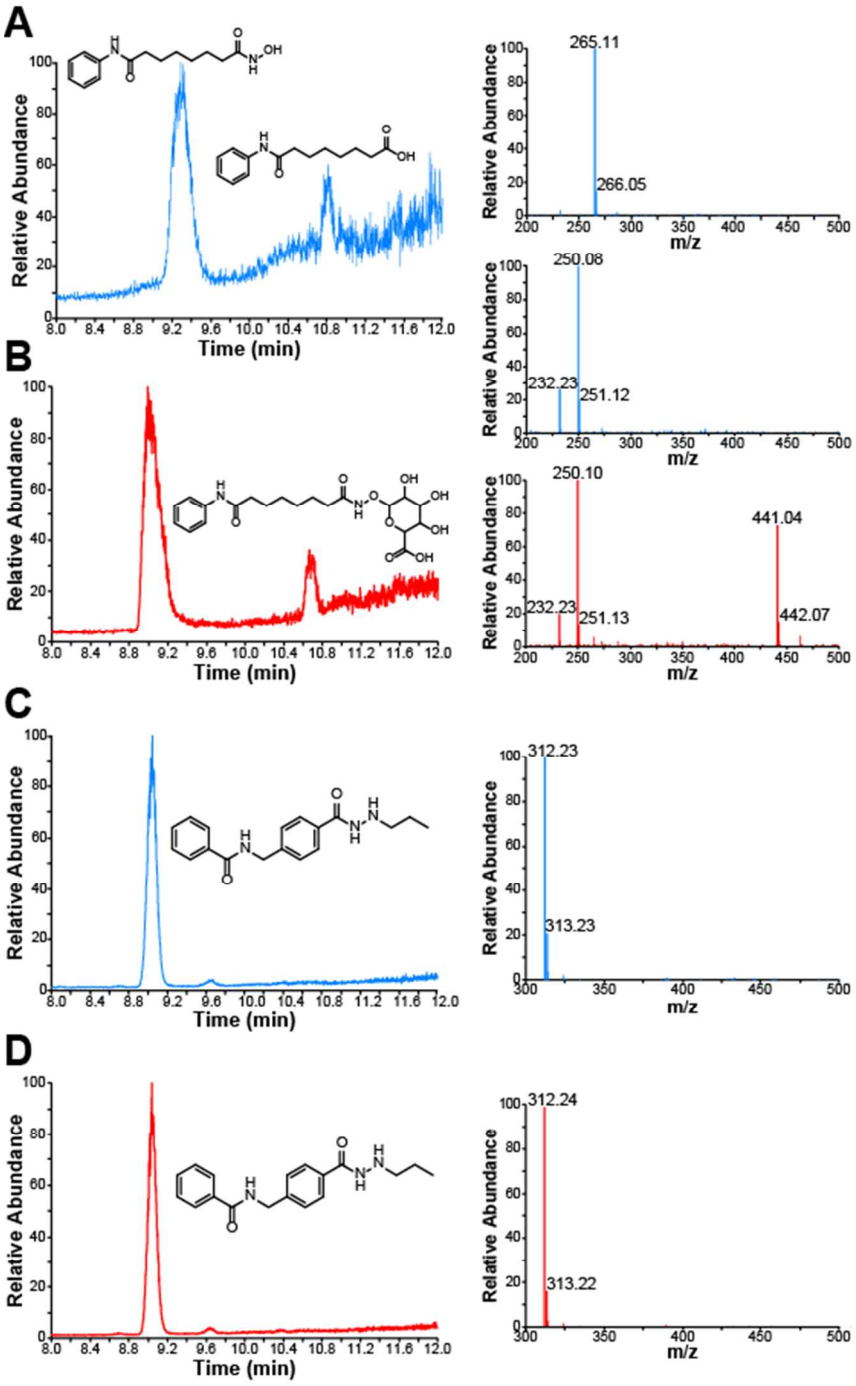

[a]ESI-LCMS TIC spectra of vorinostat incubated with human liver microsomes without UDPGA (blue, **A**) and with UDPGA (red, **B**). Both spectra contain parent compound (m/z = 265), a hydrolyzed metabolite (m/z = 250), only the UDPGA addition vessel contained the glucuronidated metabolite (m/z = 441). ESI-LCMS TIC spectra of **2d** human liver microsomes without UDPGA (blue, **C**) and with UDPGA (red, **D**). Neither vessel contained any detectable

metabolites other than parent compound. Representative spectra and mass analyses of $n \geq 3$ repeats.

Figure 2. Lineweaver-Burke plots of **2d**, **3b**, and vorinostat vs. recombinant HDACs 1 and 3[a]

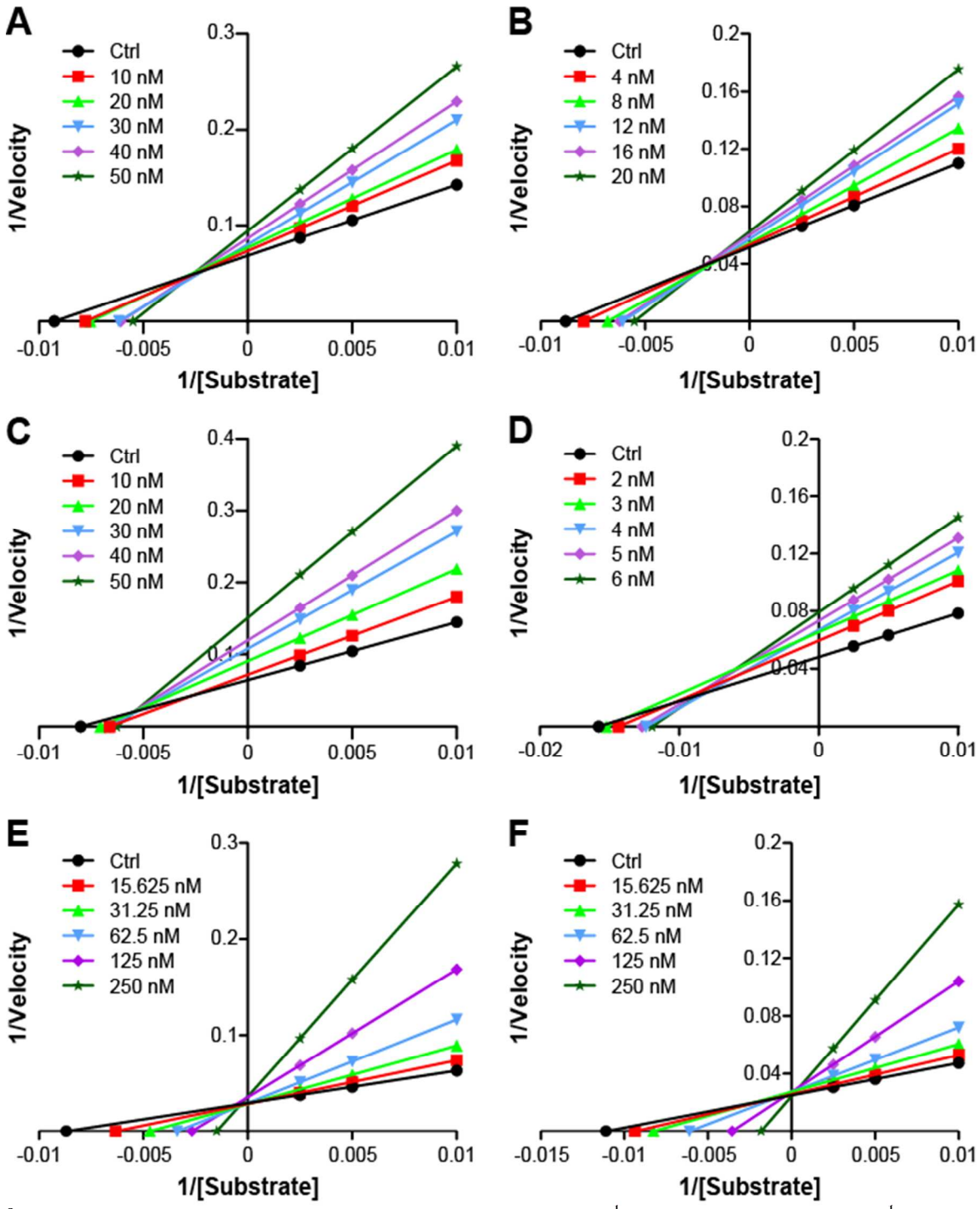

[a]Y-axes units (pmoles acetylated substrate cleaved/min)$^{-1}$. X-axes units (μmoles)$^{-1}$. **A and B) 2d** and HDACs 1 and 3 respectively. Intersection in 2nd quadrant indicative of mixed inhibition. **C and D) 3b** and HDACs 1 and 3 respectively. Intersection on x-axis and in 2nd quadrant indicative of mixed and non-competitive inhibition. **E and F)** vorinostat and HDACs 1 and 3. Intersection

directly on y-axis indicative of competitive inhibition. Representative plots of n ≥ 3 experiments.

Figure 3. Molecular modeling of **2d**, **3b**, and vorinostat against HDAC3[a]

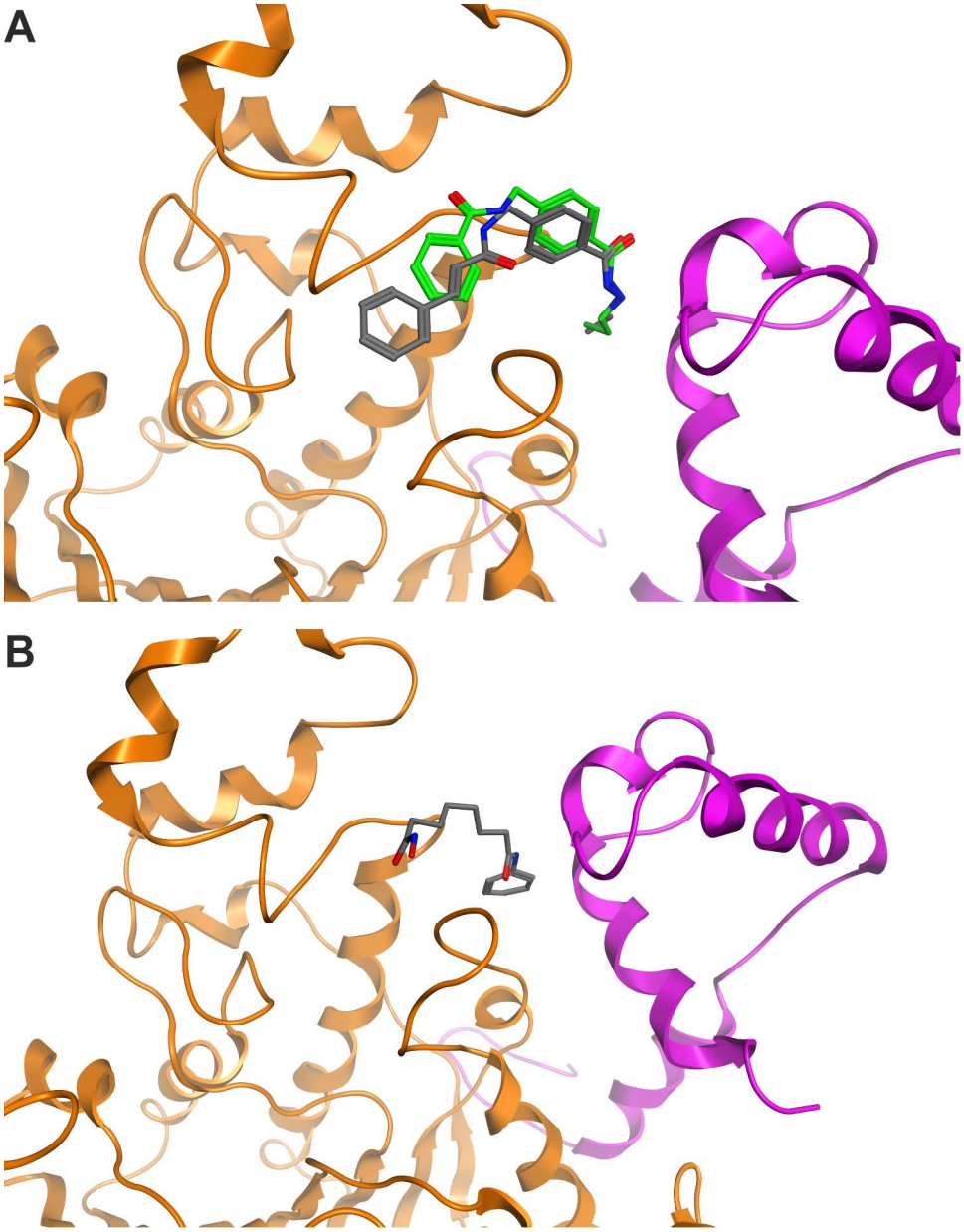

[a]**A)** HDAC3 molecular docking. PDB: 4A69 used. HDAC3 is seen in orange, Ncor2 seen in purple. Lowest binding energy poses for **2d** (green) and **3b** (carbon grey). Significant electrospatial overlap between these two poses indicative of a key pose the propyl hydrazide group is capable of conforming to. **B)** Lowest binding energy pose for vorinostat (carbon grey). Conformation has its hydroxamic acid interacting with solvent, away from a pocket, with its

phenyl group interacting with hydrophobic amino acids. This pose, and all other poses seen, possess much weaker binding interaction than lead analogs **2d** and **3b**.

Figure 4. Ex vivo analysis of lead compounds as single agents against AML[a]

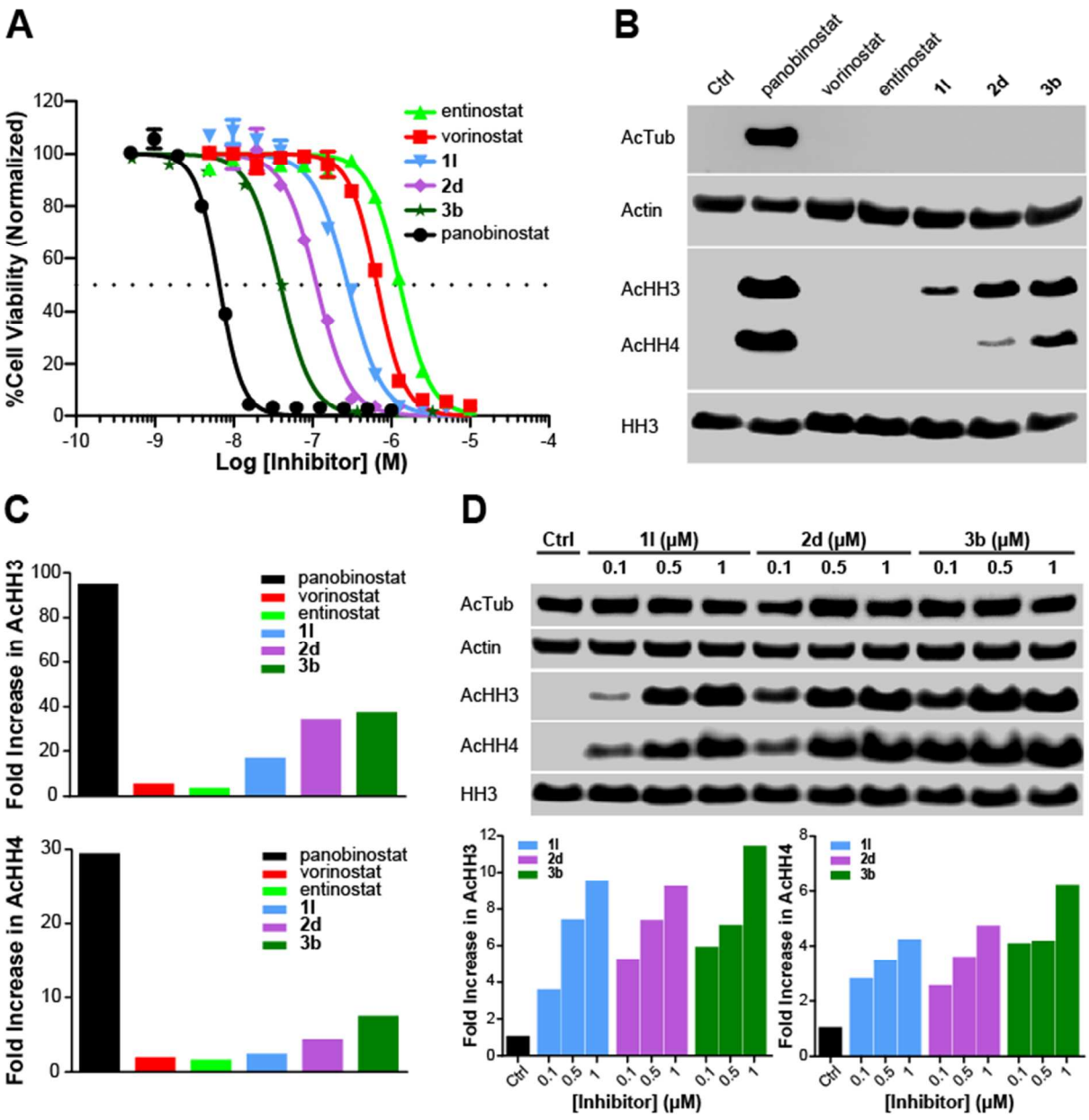

[a]**A)** EC_{50} of HDAC inhibitors against MV4-11 cells after 48 hour treatment. **1l**, **2d**, and **3b** all display lower EC_{50} values than vorinostat and entinostat, from 38-287 nM. **B)** Western blot analysis of HDAC inhibitors against MV4-11 cells at 100 nM after 24 hours. **1l**, **2d**, and **3b** cause higher upregulation of Acetylated Histones H3 and H4 (AcHH3/AcHH4) than vorinostat and entinostat. Panobinostat is the only inhibitor to raise Acetylated Tubulin (AcTub) levels at this concentration. **C)** Quantifications of AcHH3 and AcHH4 from Western blot **B**. Values normalized to actin levels. **D) (Top)** Western blot analysis of **1l**, **2d**, and **3b** at varied doses after 6 hours. All display a dose-dependent increase in AcHH3 and AcHH4. **(Bottom)** Quantification

of Western blot **D**. Values normalized to actin levels. Representative plots and blots of n ≥ 2 experiments.

Figure 5. Selectivity and toxicity profiling of lead inhibitors[a]

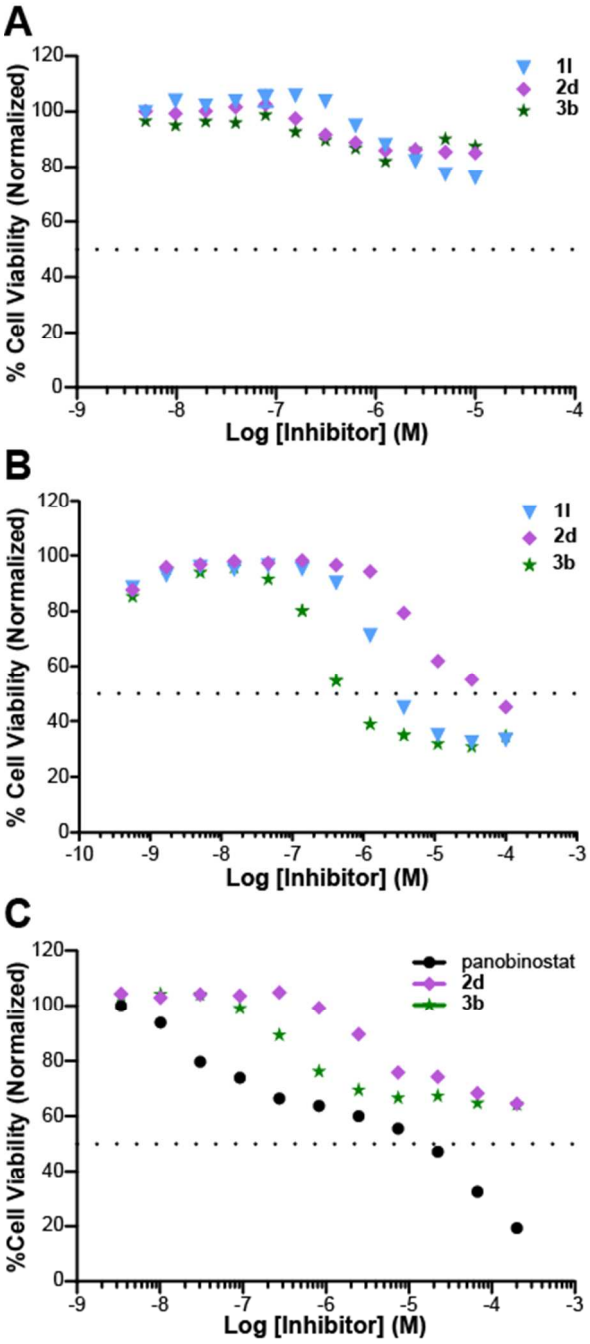

[a]**A)** EC_{50} of HEK293. Neither **1l**, **2d**, nor **3b** display effective killing of this solid tumor cell line after 48 hours of treatment. **B**) EC_{50} of HeLa. Neither **1l**, **2d**, nor **3b** display effective killing of this solid tumor cell line after 48 hours of treatment. **C)** Human PBMC profiling with panobinostat, **2d**, and **3b**. **2d** and **3b** both demonstrate superior toxicity (less PBMC killing) than

panobinostat. **2d** shows ~10 fold less toxicity than **3b** until the high micromolar range, well beyond the respective EC_{50} values of these compounds. Panobinostat displays immediate toxicity as early as 10 nM. Values normalized to vehicle treatment (DMSO). Figures are representative of $n \geq 2$ experiments.

Table of Contents graphic

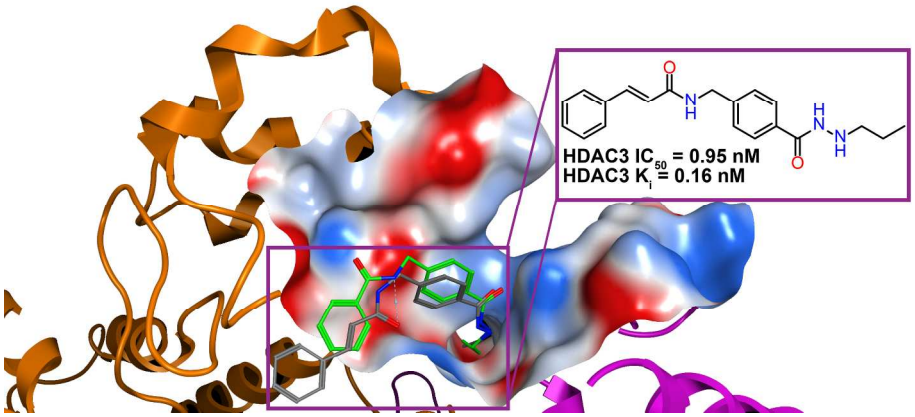

A novel series of hydrazide based class I HDAC inhibitors with low to sub nanomolar potency is described. These agents are particularly selective and deadly for Acute Myeloid Leukemia cells and represent a novel HDAC inhibitor moiety, being impervious to glucuronidation based inactivation that affects the hydroxamate containing compounds.